

University of Nebraska - Lincoln

DigitalCommons@University of Nebraska - Lincoln

Mechanical (and Materials) Engineering --
Dissertations, Theses, and Student Research

Mechanical & Materials Engineering, Department
of

Spring 5-2014

Design and Assembly of Parabolic Flight Payload to Evaluate Miniature *in vivo* Surgical Robots in Microgravity

Kearney M. Lackas

University of Nebraska-Lincoln, kearney.lackas@gmail.com

Follow this and additional works at: <http://digitalcommons.unl.edu/mechengdiss>



Part of the [Mechanical Engineering Commons](#)

Lackas, Kearney M., "Design and Assembly of Parabolic Flight Payload to Evaluate Miniature *in vivo* Surgical Robots in Microgravity" (2014). *Mechanical (and Materials) Engineering -- Dissertations, Theses, and Student Research*. 72.
<http://digitalcommons.unl.edu/mechengdiss/72>

This Article is brought to you for free and open access by the Mechanical & Materials Engineering, Department of at DigitalCommons@University of Nebraska - Lincoln. It has been accepted for inclusion in Mechanical (and Materials) Engineering -- Dissertations, Theses, and Student Research by an authorized administrator of DigitalCommons@University of Nebraska - Lincoln.

DESIGN AND ASSEMBLY OF PARABOLIC FLIGHT PAYLOAD TO EVALUATE
MINIATURE IN VIVO SURGICAL ROBOTS IN MICROGRAVITY

by

Kearney Lackas

A THESIS

Presented to the Faculty of

The Graduate College at the University of Nebraska

In Partial Fulfillment of Requirements

For the Degree of Master of Science

Major: Mechanical Engineering & Applied Mechanics

Under the Supervision of Professor Shane M. Farritor

Lincoln, Nebraska

May, 2014

DESIGN AND ASSEMBLY OF PARABOLIC FLIGHT PAYLOAD TO EVALUATE
MINIATURE IN VIVO SURGICAL ROBOTS IN MICROGRAVITY

Kearney Mathew Lackas, M.S.

University of Nebraska, 2014

Advisor: Shane Farritor

Laparoscopic surgery, also known as minimally invasive surgery (MIS), changed the face of surgery in the 1990s. With these procedures, surgeons use long, slender tools which pass through several small incisions. Performing surgery in this fashion has shown many benefits including reduced pain and recovery times, lower costs, and less scarring post-recovery.

The use of surgical robotics has shown several key advantages over MIS techniques. Minimally invasive surgeries typically require unnatural movements, have limited visibility, greatly reduce dexterity, and provide little tactile feedback. Through robot kinematics and specialized sensors, surgical robots can resolve many of these limitations, especially in terms of creating intuitive controls that can be mastered quickly, without losing many of the benefits of MIS. Because of these properties and their relatively small size, surgical robots could be viable options for use during space flight emergencies.

This thesis presents the design and assembly of a parabolic flight payload to evaluate these robots in microgravity where the robot performance and the operator capability is unknown. The structure supports all required hardware and is compliant with all NASA requirements and guidelines for microgravity research. Through future experiments using the payload, completion metrics such as

experimental time-to-completion and robot positioning accuracy will be used to define the challenges with working in microgravity as well as propose possible solutions to create a surgical system for space.

In dedication to my wife and family, for without their endless support and encouragement, I would not be where I am today.

I would also like to acknowledge my advisor, Dr. Shane Farritor, and my fellow colleagues for their guidance and contributions.

This work was performed under support provided by NASA EPSCoR, Nebraska Research Initiative, Telemedicine and Advanced Technology Research Center, and the NASA Nebraska Space Grant Consortium.

Table of Contents

Chapter 1:	Introduction.....	1
Chapter 2:	Background.....	4
Section 2.1:	Minimally Invasive Surgery.....	4
2.1.1	Standard Laparoscopic Surgery	4
2.1.2	Laparoendoscopic Single-Site Surgery	5
Section 2.2:	Robotic Surgery	6
2.2.1	Surgical Laparoscopic Surgery	6
2.2.2	Miniature <i>in vivo</i> Surgical Robots	7
Section 2.3:	Surgery in Space	8
Chapter 3:	Motivation.....	10
Section 3.1:	Overview.....	10
Section 3.2:	Experiments	10
Chapter 4:	Parabolic Flight Payload Design.....	13
Section 4.1:	Overview.....	13
4.1.1	Structural Requirements.....	13
4.1.2	Electrical Requirements	14
4.1.3	Functional Requirements	14
Section 4.2:	Equipment Descriptions.....	16
4.2.1	Robots	16

- 4.2.2 Robot Chamber 17
- 4.2.3 Computers 18
- 4.2.4 Monitors 20
- 4.2.5 Physical Input..... 21
- 4.2.6 Video Capture 23
- 4.2.7 Power Supplies..... 24
- 4.2.8 Additional Equipment 25
- Section 4.3: Structural Design and Verification 26
 - 4.3.1 Overview 26
 - 4.3.2 Assembly..... 30
 - 4.3.3 Mechanical Properties of 80/20™ Aluminum Extrusions 32
 - 4.3.4 Stress Calculation Methods..... 32
 - 4.3.5 Load Cases 34
- Section 4.4: Electrical Analysis 47
 - 4.4.1 Load Analysis and UPS Selection 47
 - 4.4.2 Emergency Stops 48
- Chapter 5: Experimental Procedures 49
- Chapter 6: Summary 53
 - Section 6.1: Future Work 55
- References..... 57
- Appendix A: 80/20™ Datasheets 61

List of Figures

Figure 1.1. Miniature <i>in vivo</i> surgical robot as seen from experiment operator's view.....	2
Figure 2.1. <i>da Vinci</i> ® Surgical System.....	6
Figure 2.2. Miniature <i>in vivo</i> surgical robot concept.....	8
Figure 3.1. Stretch-and-dissect experiment shown with EricBot 2,1.....	11
Figure 3.2. JackBot above peg transfer [14].....	12
Figure 4.1. System Schematic.....	15
Figure 4.2. EricBot 2.0 (left) and EricBot 2.1 (right)	16
Figure 4.3. Robot Enclosure	18
Figure 4.4. Rackmount Computer Case.....	19
Figure 4.5. Dell monitor with custom mounting plate attached.....	20
Figure 4.6. Mounting plate as attached to 80/20™ extrusion	21
Figure 4.7 Phantom Omni haptic device.....	21
Figure 4.8. Logitech K400 Keyboard	22
Figure 4.9. KVM Switch (left) and HDMI Matrix (right)	23
Figure 4.10. Panasonic Camcorder (left) and Universal Camera Bracket (right).....	23
Figure 4.11. Robot Power Supplies	25
Figure 4.12. Belkin Surge Protector	25
Figure 4.13. Basic dimensions of payload	27
Figure 4.14. Floor Supports	28
Figure 4.15. Assembled Payload Structure.....	29
Figure 4.16. Structure with Joint Numbers.....	31
Figure 4.17. SolidWorks Simulation	33

Figure 4.18. Mass and load location of computers and UPS	35
Figure 4.19. Lower brackets of left computer column beam	36
Figure 4.20. Downward load case beams of concern	40
Figure 4.21. Two Symmetrically Spaced Concentrated Loads.....	41
Figure 4.22. Stress Simulation of Floor Supports	44
Figure 4.23. Simulation elements with negative safety margins	45
Figure 4.24. Simulation Loading for 80/20™ Monitor Supports	45
Figure 4.25. Stress Distribution for Monitor Supports	46
Figure 5.1. Lift point with handle	49
Figure 5.2. Preferred aircraft orientation	50
Figure 5.3. Foot Restraint Bar (looking downward).....	51
Figure 6.1. Parabolic Flight Payload with EB2.1	54
Figure 6.2. Experiment performed on April 25th, 2014	55

List of Tables

Table 4.1. Computer Components	19
Table 4.2. Payload Summary	28
Table 4.3. Joint Assemblies (See Figure 4.16 for Locations)	30
Table 4.4. Acceptable Loading of 80/20™ Beams	32
Table 4.5. Acceptable Loading of 80/20™ Connectors.....	32
Table 4.6. Component Weights Used for Structural Calculations	33
Table 4.7. Summary of Structural Margins.....	34
Table 4.8. Load Table, 120VAC.....	47

Chapter 1: Introduction

Availability of effective and standard healthcare during a space flight is vital. As the duration of spaceflight increases, timely evacuation of a medically-compromised individual back to earth may not be possible. As such, many technological developments are necessary prior to any long-distance spaceflight. Among these technologies to be developed are surgical systems to perform major surgeries in microgravity.

For surgeries in a standard operating room, a transition from large, open incisions to smaller, less significant ones has occurred. Traditional open surgery offered surgeons excellent manipulation, visualization, and tactile feedback but was incredibly painful for the patient and required significant time to fully heal. Through these consequences of open surgery, minimally invasive techniques were perfected in the early 1990s. These surgical techniques offer significant benefits to the quality of care a patient receives including reduced pain, shorter hospital stays, less scarring, and even lower mortality rates [1-7]. Laparoscopy, the most well-known form of MIS in which several slender tools pass through small incisions in the abdomen, has become a routine technique to many surgeons [8]. In weightlessness, this technique would also have a great advantage over open surgery in the fact that minimal bodily fluids can escape the body cavity during operation. However, with these benefits come several consequences including unintuitive controls, the lack of depth perception, and the loss of any touch sensations.

Recently, robotic systems have been developed to mimic laparoscopic techniques but with software packages to improve the surgeons experience. The most well-known system is the *da Vinci*® Surgical System which has been approved by the Food and Drug Administration (FDA) for a variety of surgeries [9-11]. This system, however, is far too large to be flown on any near-term mission.

Previous research in the Advanced Surgical Technologies Laboratory at the University of Nebraska has demonstrated technologies that show a viable option for major surgery in microgravity. This group has developed several two-armed multi-degree-of-freedom robots [12-14]. These robots are completely inserted through an umbilical incision and have been shown to be successful in performing colectomies, cholecystectomies, and a hysterectomy [15]. It has been proposed to evaluate these robots in a microgravity environment (Figure 1.1) in preparation for further research in the area of surgical robots for space applications.



Figure 1.1. Miniature *in vivo* surgical robot as seen from experiment operator's view

Presented in this thesis is the initial design of a parabolic flight payload to be flown aboard a modified 727, owned by Zero Gravity Corporation and contracted by NASA to evaluate the robot and operator performance in microgravity. Presented first is a background of current surgical technologies used on Earth as well as other methods that have been evaluated in microgravity. Next, the motivations for this microgravity experiment will be discussed. The design and development of the console will be described. Experimental procedures to evaluate the effectiveness of such robots and supporting systems will be listed. Lastly, future areas of improvement and research, for the payload as well as the robots, will be identified.

Chapter 2: Background

Section 2.1: Minimally Invasive Surgery

2.1.1 Standard Laparoscopic Surgery

Through the late 1980s and early 1990s, a transition from traditional open surgeries to laparoscopic procedures occurred [16, 17]. Initially, this technological breakthrough was limited to simple procedures such as cholecystectomies. However, through specialized training and improved tools this technology has become synonymous with minimally invasive surgery.

During a laparoscopic procedure, slender tools are introduced into the body cavity through several small incisions. During the operation, the body is insufflated with CO₂ to increase the volume of the body cavity. Because of the positive pressure, a specialized port called a trocar is used to seal the incision against pressure loss. Visualization is achieved through the use of a laparoscope. When laparoscopic methods are used, reductions in patient pain, recovery time, and infection rates have been realized [18] largely due to smaller incision size (5-10mm vs. 20 cm).

However, these advances come with several costs. Firstly, range of motion and dexterity are largely reduced because each tool must pass through a specific point in the abdominal wall. Additionally, the motion of the tool tip is opposite to that of the surgeon's hands and scales differently with various insertion depths due to a fulcrum effect at the incision. Tactile sensation is largely eliminated and visualization, particularly in regards to depth perception, is reduced. Some of these disadvantages can be solved with sophisticated instrumentation such as the 3D Tipcam® (Karl Storz, Tuttlingen, Germany) or equipment using vibration to provide force information [19]. Devices such as these have been shown to reduce task completion time [20].

Many virtual reality (VR) training simulations are currently being developed to provide a better learning platform for MIS students as opposed to the traditional “see one, do one” apprenticeship model [21]. These simulations generate virtual renderings of the surgical environment and provide haptic feedback to mimic realistic sensations. They have been shown to increase the skills of a surgeon prior to actual surgery [22] and could be beneficial for training surgeons in dealing with microgravity [23].

2.1.2 Laparoendoscopic Single-Site Surgery

A more modern approach to minimally invasive surgery is that of Laparoendoscopic Single-Site Surgery (LESS), also known as single-port surgery. LESS is achieved through a single 2-3 cm umbilical incision through which curved tools [24] are inserted. These tools typically cross each other at the insertion to provide better angles of attack.

LESS has been shown to be feasible for cholecystectomies, appendectomies, splenectomies, nephrectomies, and colectomies [25, 26]. Delany [27] documented a reduction in the length of hospital stays from 4-6 days for an open colectomy to 1-2 days for a LESS procedure. LESS procedures are also branching out into other areas of medicine including urology [28] and gynecology [29, 30].

While performing surgery through a single incision with curved tools, triangulation, or the ability to approach a target from a desired angle, can be very difficult even for experienced surgeons. Additionally, many of the difficulties of laparoscopic surgery (visualization, scaling, mirrored movements, etc.) are present in LESS procedures as well. Specialized tools with articulating ends have helped alleviate some of these problems but much research and training is yet to come in this area of MIS.

Section 2.2: Robotic Surgery

2.2.1 Surgical Laparoscopic Surgery

As standard laparoscopic techniques progressed, researchers attempted to provide assistance to surgeons through the use of robotics. The first example was the Automated Endoscopic System for Optimal Positioning (AESOP) [31]. With AESOP, the surgeon was capable of controlling the endoscope with his voice.

Since then, the process of automating laparoscopic tools has led to many versions of robotic laparoscopic surgery systems which have the potential to provide intuitive control and high precision without sacrificing the benefits of MIS [32]. These systems can combine highly scaled movements with magnified views to perform surgeries that would otherwise be extremely difficult.



Figure 2.1. *da Vinci*® Surgical System

Currently, the *da Vinci*® Surgical System (Figure 2.1), developed by Intuitive Surgical, is the most advanced robotic system and is the only system approved by the FDA [33]. Competing platforms include Raven [34], CoBRASurge [35], MC²E [36], and MiroSurge [37]. These robots are smaller in size and cost significantly less but are less capable. Also, because these platform are not FDA-approved, they are used mainly as research platforms to test a variety of new functionality including haptic feedback [38] and remote collaborative surgery [39].

2.2.2 Miniature *in vivo* Surgical Robots

In contrast to the robotic laparoscopic systems, *in vivo* surgical robots are fully inserted into the body cavity. Though the body cavity is insufflated with CO₂ to increase volume, the robots still must be very small. The robots can be either mobile or can be fixed relative to the operating table. An incision across the navel is a typical point of access similar to that of LESS surgeries.

The Advanced Surgical Technologies Laboratory at the University of Nebraska has demonstrated several versions of such robots. These robots consist of two multi-DOF arms with either a grasper or monopolar cautery at the tooltip [12, 13, 15]. They pass through a special trocar inserted into an umbilical incision (Figure 2.2). They are then fixed to the operating table. Once inside the body cavity, these robots have shown capability in performing surgery in all four quadrants of the body cavity [14]. It is these such robots that are proposed for minimally invasive surgery in space and will be evaluated through NASA's Reduced Gravity Program.

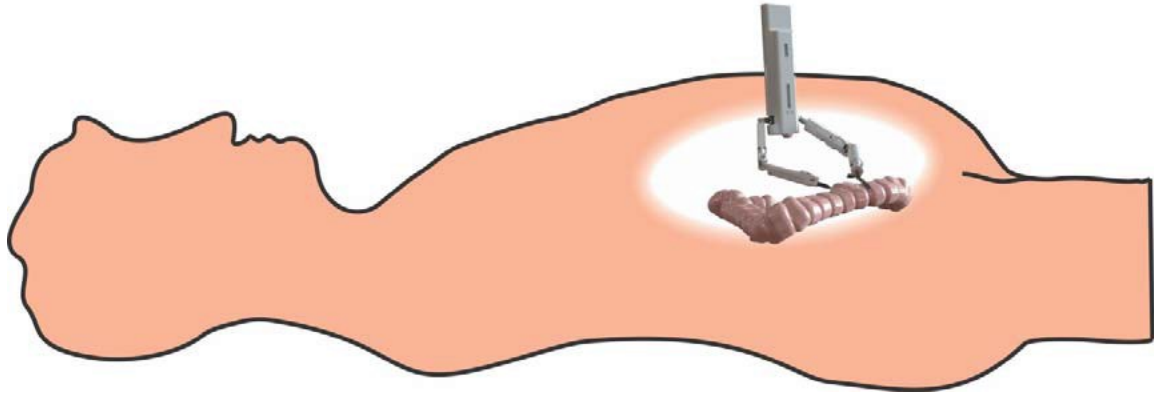


Figure 2.2. Miniature in vivo surgical robot concept

Section 2.3: Surgery in Space

As space technologies have increased, the possibility for a long-term space flight has also increased. With long-term space flight comes the potential for medical emergencies requiring intervention. However, no system yet has been shown to be a viable option for surgery in space.

In the last decade, an attempt to transfer laparoscopic techniques to microgravity has been undertaken [42]. Panait [43] concluded that while task completion rates were reduced in microgravity, there is no barrier to effective laparoscopic surgery. Rafiq [44] studied microgravity effects of on fine motor control, determining that force control and movement accuracy were noticeably reduced. Lastly, Kirkpatrick [45] observed that visualization during MIS techniques in microgravity was actually improved due to bodily fluids and debris clinging to the abdominal wall through surface tension. One challenge of the MIS approach is that the operator must be sufficiently trained in order for the surgery to be successful. Given the difficulty of MIS in 1-g, virtual reality simulations of microgravity surgery have been proposed as training tools for astronauts who may not have had any prior experiences performing in weightlessness [23].

It has been proposed recently that robots developed at the University of Nebraska will be capable of performing surgery in weightlessness [46]. These robots have the advantage of an easier learning

curve. The kinematics of the robot take care of mismatched movements allowing the surgeon to concentrate on what he means to do instead of how he needs to move. Additionally, robots such as these are extremely small (under a kilogram in mass). Additionally, the operator of the robot can be seated and stabilized in an ergonomic and stable position away from the table instead of being required to be “leaning” over the operation.

Chapter 3: Motivation

Section 3.1: Overview

The performance of miniature *in vivo* robots needs to be evaluated in microgravity where several parameters of the robot as well as the operators will be studied. In analyzing the robot, accuracy studies will be the most influential. In standard gravity, any backlash in the robot will typically fall to a gravity-neutral position. In weightlessness, there is no forces to stabilize the joints and it may be realized that the tooltips will oscillate throughout the surgery. This can be solved by elastic compensation at the joints if these mechanics are realized through microgravity experiments.

In analyzing the operators, task completion percentages and completion times will be used to infer performance. In microgravity, it has been documented that fine motor control is reduced [44]. This effect has yet to be seen when controlling a haptic device which is capable of providing reaction force. Additionally, methods to stabilize the operator can be determined for subsequent flights.

Section 3.2: Experiments

Throughout the flight a series of experiments can be performed. The main experiment to evaluate performance will be that of a stretch-and-dissect procedure. The stretch-and-dissect experiment (Figure 3.1) challenges the operator to grab one side of a marked rubber band. Once a successful grasp is achieved, he will cut along the mark, separating the two halves. In subsequent attempts, the operator may grasp the free end of a previously cut rubber band to stretch it and make a second cut.

This experiment challenges the system in a variety of ways. Firstly, it tests the accuracy of grasping as well as cutting. In these attempts, depth perception may be challenging due to the two-dimensional vantage point. Other visual cues such as shadows may be required. Secondly, once the cut is made the elasticity of the rubber band will provide insight into the rigidity of each arm as

well as the stability of the motor controllers. Lastly, attempting to grasp a free floating object will be challenging through the requirements of very fine movements and accurate positioning. Any attempts without these aspects will fail at grasping free-floating objects.

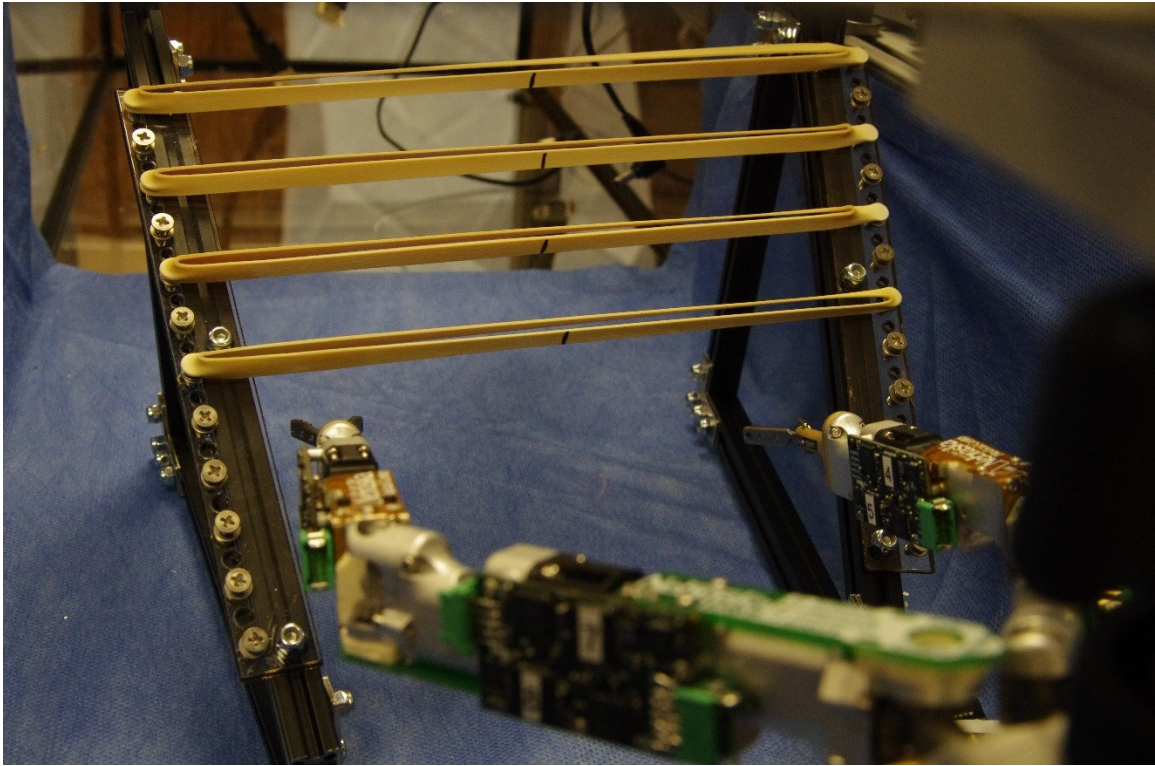


Figure 3.1. Stretch-and-dissect experiment shown with EricBot 2,1
Note: EricBot is described in Section 4.2.1

The microgravity manipulation experiment (Figure 3.2) uses a standard laparoscopic training tool in microgravity. The challenge is to grab a foam sleeve, transfer the sleeve to the opposite hand, and place the sleeve on an unoccupied peg. This experiment also challenges the ability to make fine, deliberate movements while maintaining accurate positioning. Because this task requires a grasper on each hand, this task is incompatible with robots that have dual graspers.

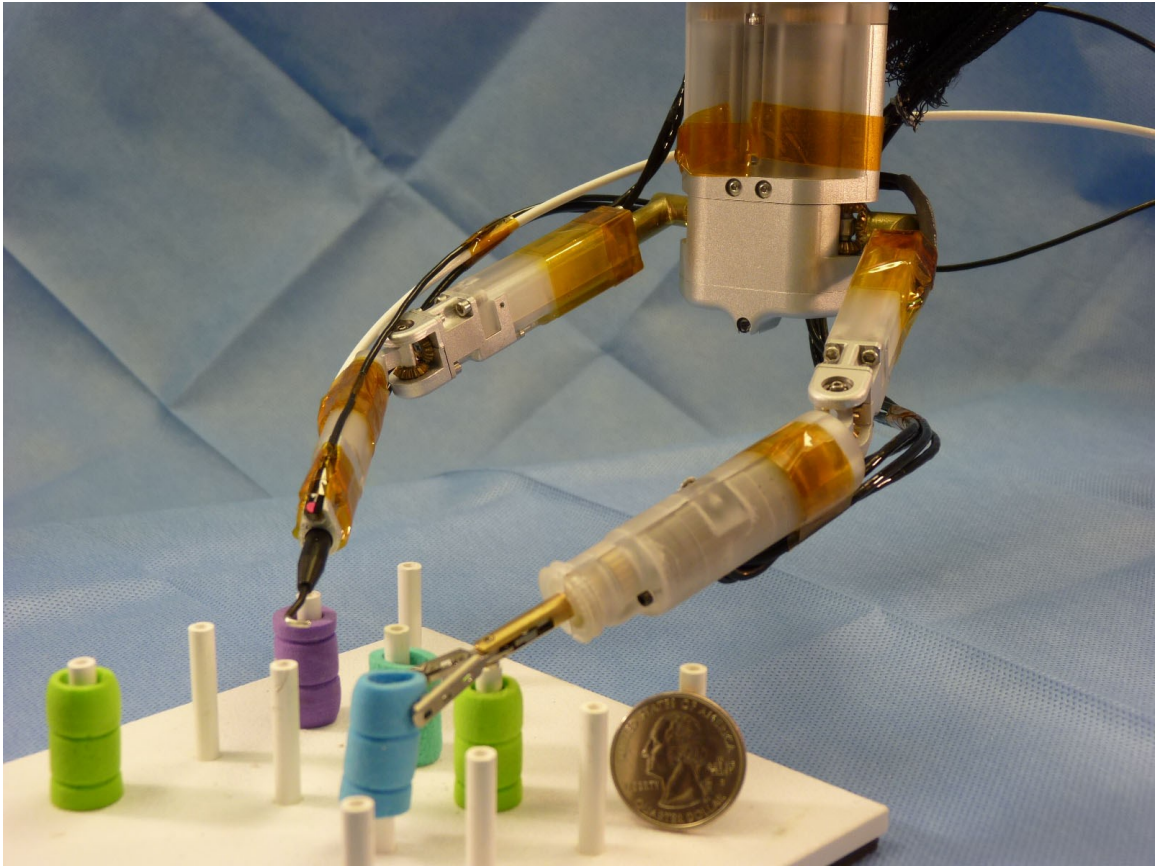


Figure 3.2. JackBot above peg transfer [14]

Note: JackBot (JB1) was developed by Jack Mondry at the University of Nebraska in 2012.

Chapter 4: Parabolic Flight Payload Design

Section 4.1: Overview

The following section provides a basic description of the test equipment design requirements and guidelines that must be met for flight on NASA's Reduced Gravity Aircraft. Compliance with these requirements is evaluated prior to flight at the Technical Readiness Review (TRR). Further details can be found in NASA documentation [47-50].

4.1.1 Structural Requirements

Structural integrity of all equipment flown aboard NASA's Reduced Gravity Aircraft must be verified. Factors of Safety (FS) of 2.0 or greater shall be applied to all structural elements. Any standard method of analysis can be used to verify structures. Material yield strengths are to be used as the maximum allowable throughout all design calculations per the requirements of NASA

All test equipment including fasteners, individual components, frames, full assemblies, and enclosures must be designed to withstand the following g-loads during take-off and landing.

- Forward: 9-g
- Aft: 3-g
- Down: 6-g
- Lateral: 2-g
- Up: 2-g

Experimental equipment must also consider in-flight load cases. During the parabolic flight, the equipment will experience g-load transitions from 0-g up to 2-g. Additionally, equipment must be capable of withstanding inadvertent contact loads from floating individuals.

Test equipment fastened to the floor using bolts must possess a frame or baseplate that matches the floor attachment grid in the aircraft test cabin. Floor attachment holes in the experiment base plate must be centered on a 20 ± 0.05 inch square pattern with holes drilled using a recommended clearance hole. No more than four anchor points may be used per payload.

4.1.2 Electrical Requirements

Each experiment must have emergency shutdown capabilities. The preferred method is a single “kill switch” located in an easily accessible location. This “kill switch” must de-energize all components in the system to a safe state, including hardware powered by an auxiliary source or an Uninterruptible Power Supply (UPS). This capability must be demonstrated at the TRR.

In the event of electrical power loss, all experiments must fail to a safe configuration. There will be a brief interruption of electrical power during engine startup and momentary interruptions of electrical power may occur during flight. Test equipment should incorporate protection devices such as a UPS to prevent data loss.

Experiments must provide an electrical cable to reach a power distribution panel. All power cords should be 20 feet in length and have a descriptive tag secured to the end stating the voltage and maximum current required. Internal cabling must be restrained and clamped and the payload must be grounded to prevent electrical shock. The experiment should be self-protected with an incorporated circuit breaker or other current-limiting devices.

4.1.3 Functional Requirements

To evaluate UNL’s *in vivo* surgical robotics, several functional requirements were determined. Equipment descriptions will be found in the following sections.

For the parabolic flight, two robot designs are to be tested – EricBot 2.0 (EB2.0) and EricBot 2.1 (EB2.1), both designed at the University of Nebraska by Eric Markvicka [51]. The robots should

be isolated from the rest of the payload 1) to prevent any inadvertent contact with the robots during microgravity and 2) to contain any small free-floating components that are either from the experiment or are debris from a mechanical failure. The chamber is to be easily accessible if an individual needed to move a component or swap an experiment.

During operation it is desired that two individuals are capable of controlling robots at the same time. This required four total haptic devices and two independent computer systems. It was decided to add a third system to assist the prior two during operation by monitoring diagnostic information and to assist troubleshooting potential problems. A KVM switch is used to provide mouse and keyboard support to all three systems from a single location. Live visual information was obviously required to view the robots. Two viewpoints were requested through which an HDMI matrix was used to manage the feeds. A schematic of data and connections similar to what is shown in the Figure 4.1 was used to select components and design the payload.

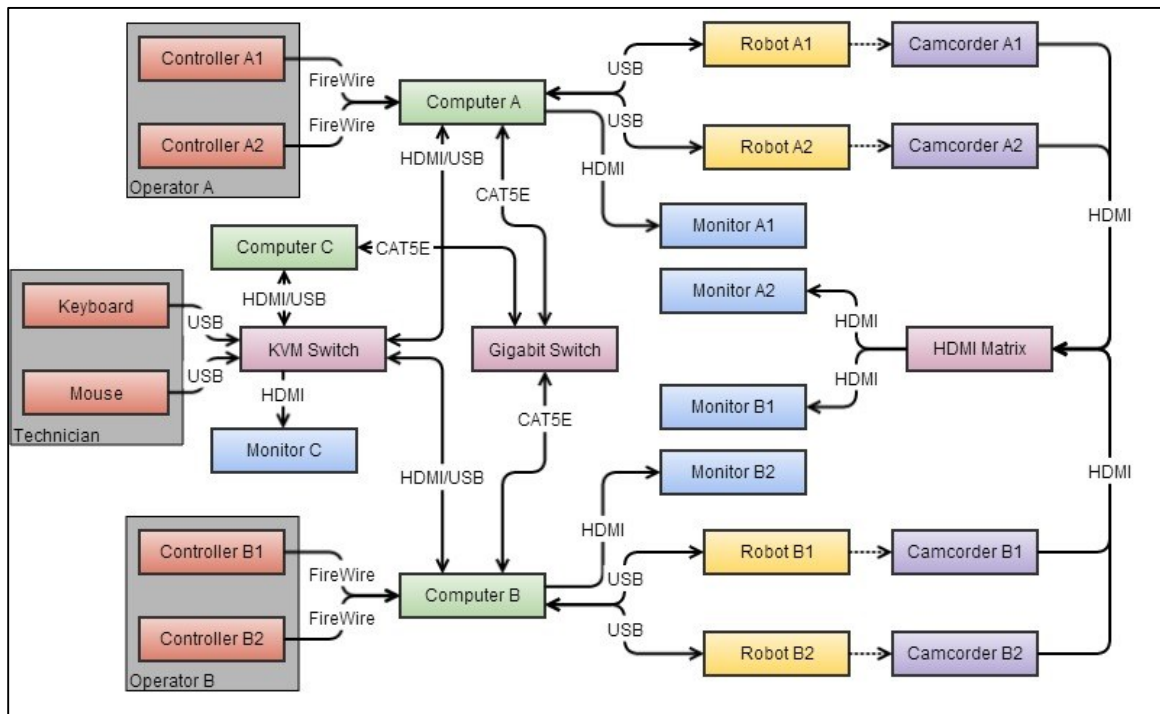


Figure 4.1. System Schematic

Section 4.2: Equipment Descriptions

4.2.1 Robots

Two robots versions of EricBot (EB) are to be flown. Each version is of approximately equivalent size and weight. They both incorporate distributed motor control systems for brushless motors; the bulk of this hardware was developed by Bartels [41]. Each joint requires a small printed circuit board (PCB) including a microcontroller, motor driver, and feedback method. Each PCB is directed by a master board located elsewhere. This master board receives commands from the Robot Operating System (ROS) (see Section 4.2.3), directs them to each respective joint PCB, or slave, collects joint statuses, and returns this global robot status back to the Robot Operating System.

From a mechanical standpoint, the two versions of Eric Bot, EB2.0 and EB2.1 are almost identical. The kinematic structures of each robot is identical and both are constructed from machined aluminum and plastic with stainless steel machine screws. EricBot 2.1 was designed with slightly larger motors in the body but arm motors are the same.

In terms of electronics, the robots are more dissimilar. Circuit boards between the two are different in layout. EB2.1 uses more advanced cabling techniques such as flexible PCBs and custom flexcables. Small and robust Gecko connectors were also used and all circuitry was exposed.



Figure 4.2. EricBot 2.0 (left) and EricBot 2.1 (right)
Note: EB2.0 is not shown with wiring between joints.

4.2.2 Robot Chamber

The robot chambers (Figure 4.3) are constructed with MakerBeam™ aluminum extrusions. These extrusions are similar to 80/20™ extrusions but are less than half the size. Joints are created through 90° stainless steel plates and special M3 screws that slide within the extrusion.

The chamber is sealed using 3mm clear polycarbonate panels that slide within the grooves of the extrusion. A hinged access door is available to insert and remove the robots and camcorders. Access holes are created where cable pass-throughs are necessary. With the exception of these cables, nothing will be able to enter or exit the chamber while the access panel is closed.

Robots, camcorders, and experiments are all supported by an 80/20™ extrusion that passes through the chamber to provide more rigidity. The only loads applied to the MakerBeam™ structure are those generated from chamber's own weight.

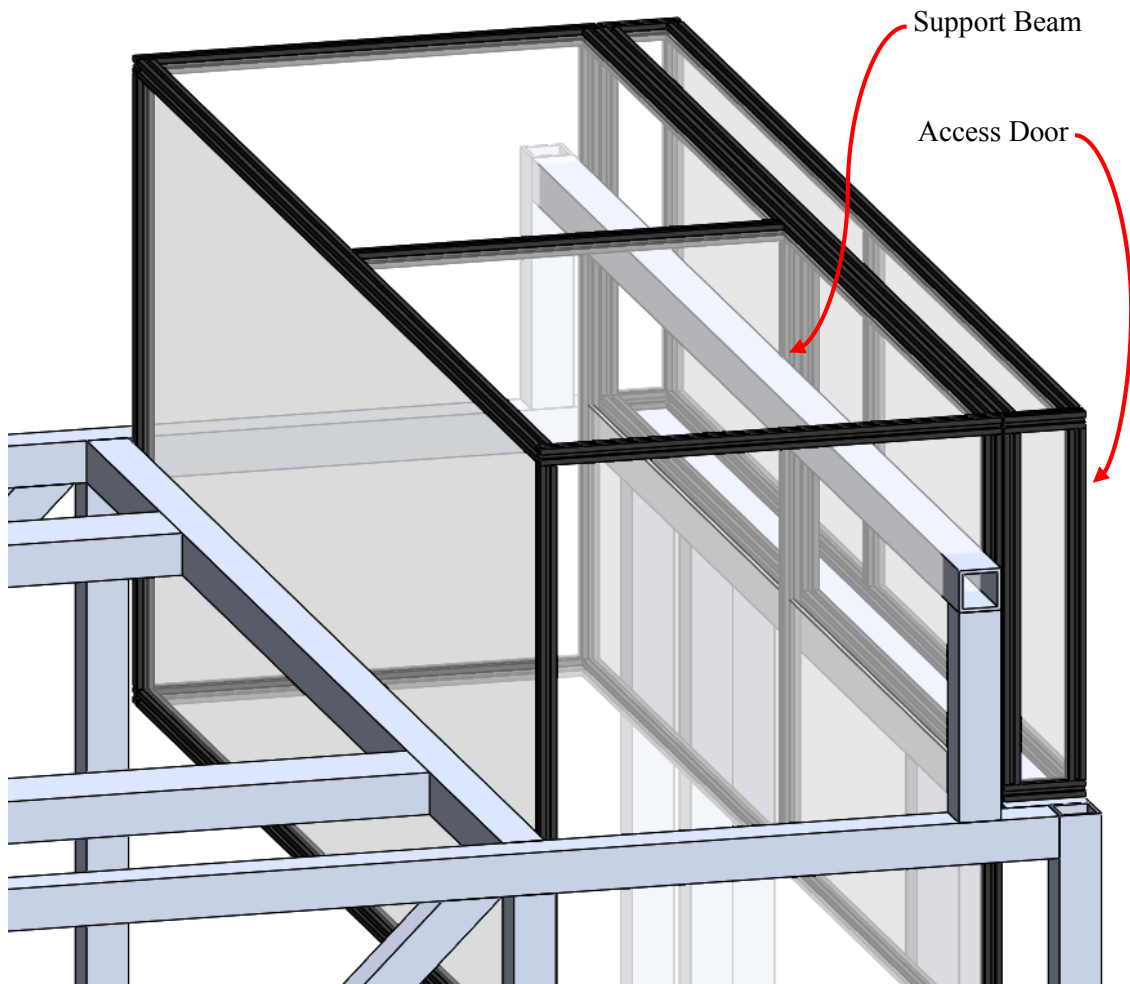


Figure 4.3. Robot Enclosure

4.2.3 Computers

The flight console will incorporate three identical 64-bit Ubuntu computers – two for robot operation and one for assistance and troubleshooting. A build table for these computers is shown in Table 4.1. All components are housed in 18 inch rack-mount computer cases (Figure 4.4) located towards the bottom of the payload to keep the center of gravity as low as possible. Each complete computer weighs 10 kg.

Table 4.1. Computer Components

Component	Brand	Description
CPU	Intel	i7-4770k
Motherboard	ASRock	Z87 Extreme6
Memory	G.SKILL	Ripjaws X Series 16 GB
Storage	Samsung	840 Pro Series 128GB SSD, RAID 1
Power Supply	Antec	EarthWatts 380W
FireWire Card	BYTECC	BT-FW310LV
Case	Norco	RPC-250

**Figure 4.4. Rackmount Computer Case**

All computers and robots communicate through the Robot Operating System (ROS). In this fashion, robots are not necessarily installed to a single machine but instead are installed to a collective pool of computing power. This provides versatility against hardware and/or software problems by allowing control of any robot through any computer at any time.

4.2.4 Monitors

The flight system will incorporate a total of five Dell 1703FP LCD Monitors (Figure 4.5). These 17 inch monitors weigh approximately four kilograms each and are rated for 55 watts of power. Each robot operator will have a pair – one for visual feedback to control the robot and a second to display live diagnostic information. The fifth monitor will be used by an assistant to help the operators with control, strategy, and troubleshooting mid-flight.

Monitors will be mounted to the payload with a custom plate (Figure 4.6) that adapts the 100mm VESA mounting pattern located on the back of the monitor to an 80/20™ compatible pattern.



Figure 4.5. Dell monitor with custom mounting plate attached

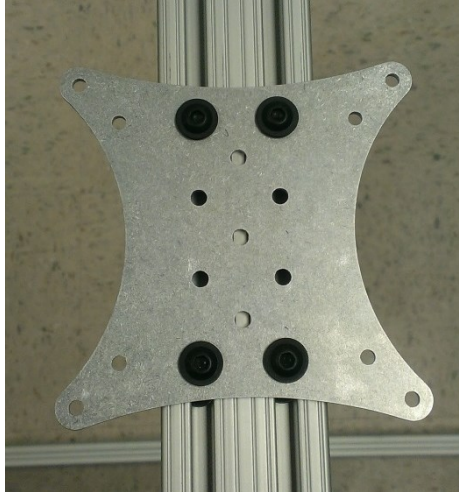


Figure 4.6. Mounting plate as attached to 80/20™ extrusion

4.2.5 Physical Input

To manipulate the arms of each robot, a total of four Phantom® Omni haptic devices are used – one for each arm of each operator. This 6-DOF physical input device captures the three-dimensional position and orientation of its stylus and provides 3-DOF haptic feedback in Cartesian coordinates to the operator's hand. The devices do not provide rotational haptic feedback. A pair of momentary switches on the pen provide additional input. These are assigned to open and close the surgical robot grasper.



Figure 4.7 Phantom Omni haptic device

The haptic functionality of the Phantom Omnis has been shown to be effective in constraining the user to the robot's workspace [41]. Additionally, the movements of the operators can be scaled before being executed at the robot level. This can provide highly accurate positioning during the surgical procedure. Lastly, though not currently developed for either version of EricBot, software limits could be programmed in the future to prevent the arms from colliding with each other.

Because these devices are meant to rest on a tabletop, a custom mounting solution was required. Modifications to prior brackets were made to provide compatibility with 80/20™ extruded aluminum profiles. With brackets installed, each device weighs 2.5 kg and is secured with four ¼-20 countersunk steel screws.

A Logitech K400 wireless keyboard was installed to provide traditional keyboard-and-mouse input to the computers. The K400 keyboard was chosen for its integrated track pad. This feature eliminated the need for a traditional computer mouse which would have been required to be free during operation but stowed for safety reasons when not in use – an unnecessary procedure which would have likely been performed several times throughout the flight.



Figure 4.8. Logitech K400 Keyboard

Through an IOGear KVM (Figure 4.9), an assistant will be able to bring up the diagnostic information presented on other monitors and control any computer using the single keyboard described above.

The addition of a Monoprice HDMI matrix (Figure 4.9) allows all video feeds to be displayed on any monitor. This is switched by a technician through a simple button press. For any future flights, control of the matrix can be programmed into ROS through an RS485 connection.



Figure 4.9. KVM Switch (left) and HDMI Matrix (right)

4.2.6 Video Capture

Five Panasonic HC-V110 digital camcorders (Figure 4.10) will be used to record footage of the experiment. Within the robot chamber, one camcorder will provide a downward view for each robot while a third and fourth will provide off-axis views to determine depth. Each camcorder will be supported by a ball socket camera bracket (see Figure 4.10). An additional camera will be placed outside the payload to capture in-flight footage of the crew.



Figure 4.10. Panasonic Camcorder (left) and Universal Camera Bracket (right)
Note: Images are not to scale

4.2.7 Power Supplies

4.2.7.1 UPS

An Uninterruptible Power Supply (UPS) is used for all components. In this fashion, transition periods during transportation of the console or interruptions of power during flight will not cause the system to forcefully power down. Also, because all components pass through the UPS, its power button becomes a system kill-switch in the case of an emergency. Electrical specifications will be described in Section 4.4.

It is possible through an RS485 or USM connection between the UPS and the Robot Operating System to command the computers to perform some actions based on the status of the UPS. For example, if no input power is present and the UPS is at a low capacity, the computers can be automatically signaled to safely shut down. These features have yet to be programmed but could be easily implemented for future flights.

4.2.7.2 Robot Power

Three power supplies will be used for the robots. These include 12V and 9V supplies for motor power and a 5V supply for logic power. The 12V and 9V supplies are passed through an emergency stop located within reach of either operator. The logic supply is not to be interrupted. The power supply package that was chosen was that of a standard laptop charger (Figure 4.11). These supplies are completely sealed and are thus immune to damage due to floating debris during microgravity.



Figure 4.11. Robot Power Supplies
Note: Objects are not to scale

4.2.8 Additional Equipment

Several additional components are required for operation. Firstly, a Belkin 12-Outlet Surge Protector (Figure 4.12) is used to expand the number of power outlets. This is located at the top of the structure near the monitors, haptic devices, and camcorders. All twelve outlets are used. A TRENDnet TEG-S50g gigabit network switch is used to network all computers together.

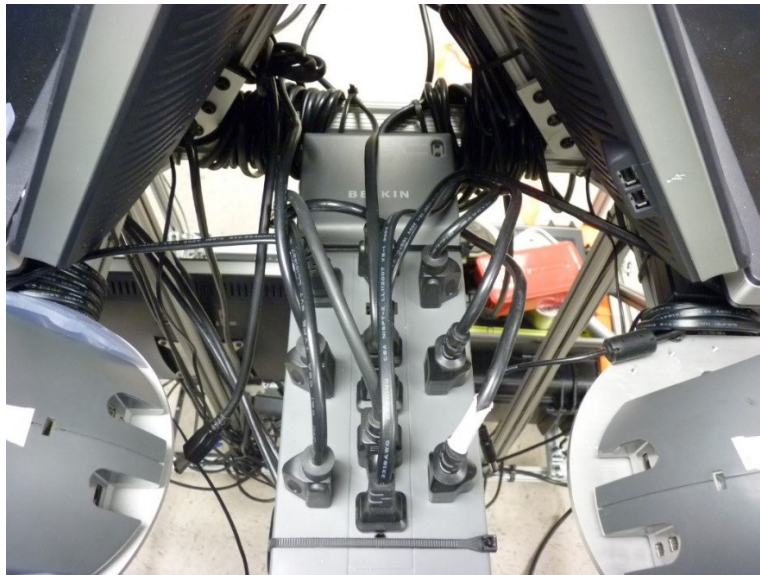


Figure 4.12. Belkin Surge Protector

An accelerometer attached to an Arduino Uno is used to measure acceleration. This data stream is passed through USB into the assistant computer. Within the ROS network, this data is published

for other nodes to use if necessary. Additionally, this acceleration is time stamped to match that of robot diagnostics. From the Arduino UNO, an LED within the robot enclosure will illuminate during microgravity. This allows the ROS data to be synced with the video footage during post-analysis.

Section 4.3: Structural Design and Verification

4.3.1 Overview

In designing the structure (Figure 4.13), several factors had to be considered. First, the locations of monitors and haptic devices were placed at a comfortable height. This set the height of the payload to be 36 inches above the floor. The haptic devices are secured to the bases through ten #8 screws while the base is secured to a double wide 80/20™ beam through four ¼-20 screws. Monitors are secured to 80/20™ beams through ¼-20 screws and a custom monitor support bracket. The beams supporting the angled monitors can be adjusted to meet the needs of various operator heights. The power supply is mounted on its own beam located between these monitors as seen in Figure 4.12.

Through the dimensions of the robots and their workspaces, it was determined that eleven inches of chamber width was sufficient if the robots were orientated in the same direction as the operators. This is to say that the robots would face each other. As mentioned earlier, the cameras and robots are secured on an 80/20™ beam that passes through the chamber. This height of this beam is set three inches below the polycarbonate to provide clearance for the downward facing camcorders.

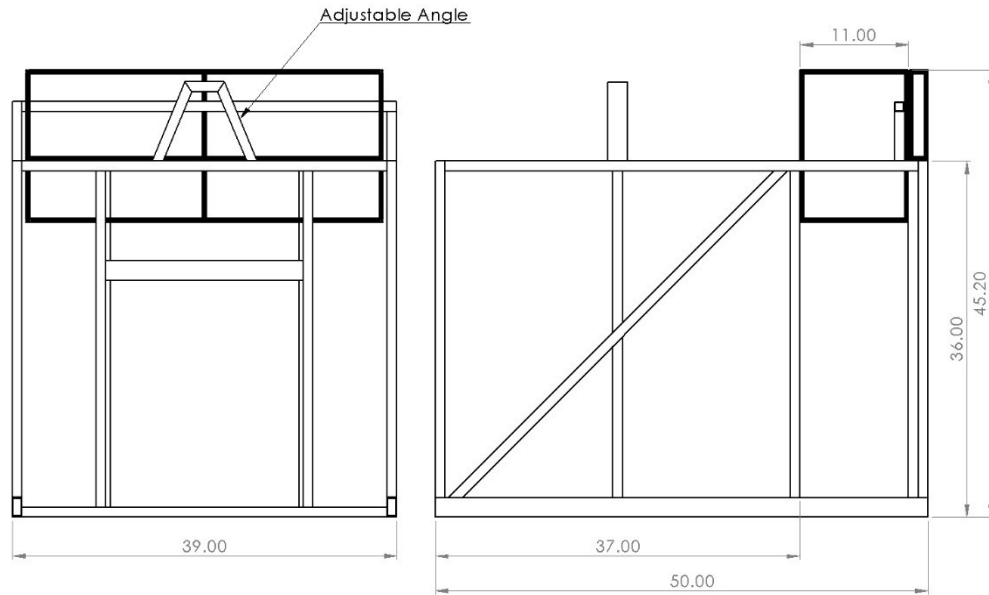


Figure 4.13. Basic dimensions of payload
Note: All dimensions in inches

The width of the monitors, haptic devices, and robot chamber set the width of the entire payload to 50 inches. Because this is incompatible with the 20" x 20" repeating bolt pattern, it was decided that the depth must be compatible with the pattern while the location of the supports along the width of the payload would be adjustable. Custom floor supports (Figure 4.14) were machined from 7075-T6 aluminum. The mounting surface is $\frac{1}{2}$ inch from the centerline of the floor bolt. Therefore, the depth of the payload must be 39 inches to match the aircraft's bolt pattern. Structural simulation of the floor support is found in following sections.

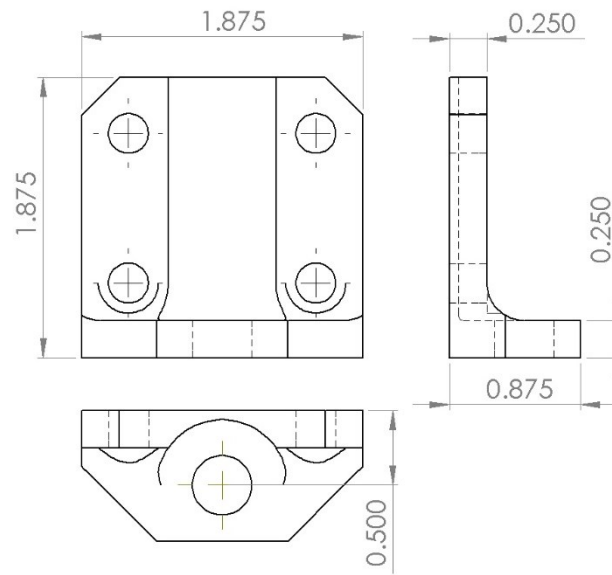


Figure 4.14. Floor Supports

Double 80/20™ beams were used to mount the computers for two reasons. Firstly, the additional strength is needed as the computers are some of the heaviest components in the payload. Secondly, this slightly recesses the computers in the payload, reducing the chance of accidental contact with power buttons.

A diagonal beam was installed on each side to resist translational loads. As one will see in following sections, loads in this direction are most significant and these beams become integral to the rigidity of the payload. All other beams were designed to complete the structure through sufficient stiffness, strength, or mounting capability. Table 4.2 shows a summary of the payload, and an image of the assembled structure is shown in Figure 4.15.

Table 4.2. Payload Summary

Parameter	Value
Payload Area	13.54 ft ²
Working Area	50 ft ² (approx.)
Height	46 in
Weight	275 lb (approx.)
Height of CG	18.70 in
Aircraft Loading	18.5 lb/ft ²



Figure 4.15. Assembled Payload Structure

Note: The equipment installed on the structure is different than what is specified throughout this thesis. The structure, however, is identical and the casters are removed for the experiment

4.3.2 Assembly

During assembly, 4-hole gusset connectors were used wherever high loads were experienced. Where possible, additional 2-hole gussets and anchors were used to create a very rigid joint. Joint information is shown in Table 4.3.

Table 4.3. Joint Assemblies (See Figure 4.16 for Locations)
A - Anchor, DG - Double Gusset, SG - Single Gusset, 90P - 5 Hole 90° Plate, 45P - 4 Hole 45° Plate

Joint Number	X-Y Plane	X-Z Plane	Y-Z Plane
1	1x A, 1x DG	1x SG	1x A, 1x DG
2		2x SG	
3			2x 45P
4	1x SG	1x A, 1x SG	1x A, 1x DG
5	1x DG	1x SG	1x A, 1x DG
6	1x 90P		
7	2x 90P		
8	1x DG	1x SG	1x DG
9	1x SG	1x A, 1x SG	1x A, 1x DG
10	1x SG	1x A, 1x SG	
11	1x DG	1x SG	1x A, 1x DG
12	2x 45P		
13	2x SG		
14	2x SG	2x SG	
15		2x SG	
16		2x SG	
17	2x SG	4x SG	2x SG
18		2x SG	
19			1x SG
20	1x SG		

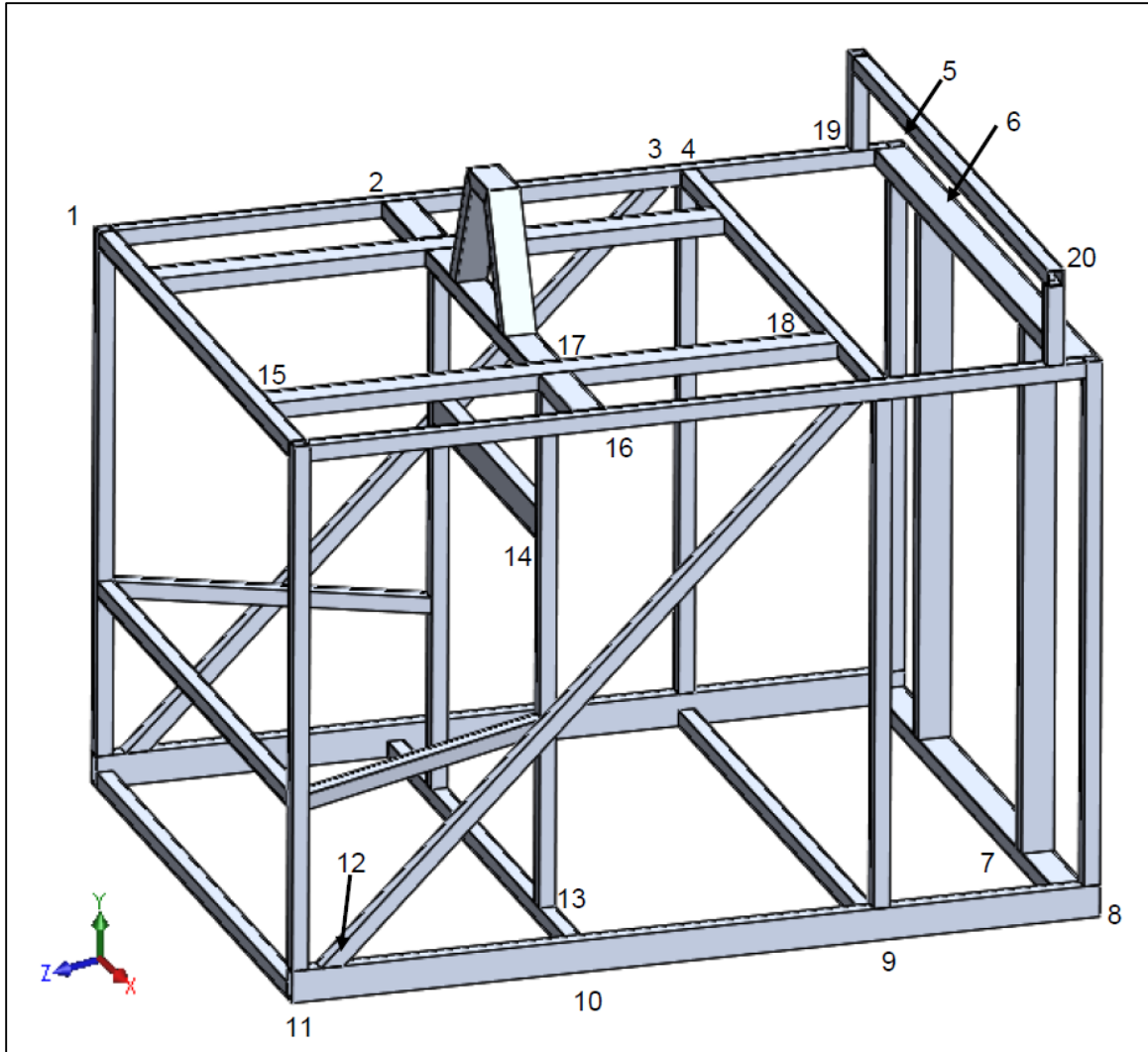


Figure 4.16. Structure with Joint Numbers
Note: The payload is symmetric about the Y-Z plane

Using a digital torque wrench, all fasteners were tightened to five ft-lbf per manufacturer specifications. This torque is claimed to be high enough to preload the T-nuts into the 80/20™ extrusions while preventing the screws from vibrating loose. Torques higher than this create the potential of weakened threads or tool damage. At a load beyond five ft-lbf, a ball hex socket broke within the head of a button cap screw. A hacksaw was required to remove the tightened screw – an unnecessary consequence of over-tightening.

4.3.3 Mechanical Properties of 80/20™ Aluminum Extrusions

Table 4.4. Acceptable Loading of 80/20™ Beams

Beam	Moment of Inertia (x10 ⁻⁹ m ⁴)	Allowable Moment (Nm) ¹
1010	18.40	174.8
1020	34.67	329.4
	128.12	608.6

¹ Maximum Moment was determined by solving the standard bending stress equation for the moment required to generate 50% of the yield stress. From [57], the yield stress for 80/20™ extrusions is 241.3 MPa (35,000 psi).

Table 4.5. Acceptable Loading of 80/20™ Connectors

Load Condition ¹	Anchor	90° Joining Plate	2 Hole Corner Gusset	4 Hole Corner Gusset ²
Allowable Shear Force	1112 N	389 N	723 N	1446 N
Allowable Bending Moment	70.7 Nm	14.2 Nm	62.2 Nm	124.4 Nm
Allowable Torsion	10.2 Nm	28.2 Nm	14.7 Nm	29.4 Nm

¹ These are loads stress the connector to 50% of the load at which it would fail.

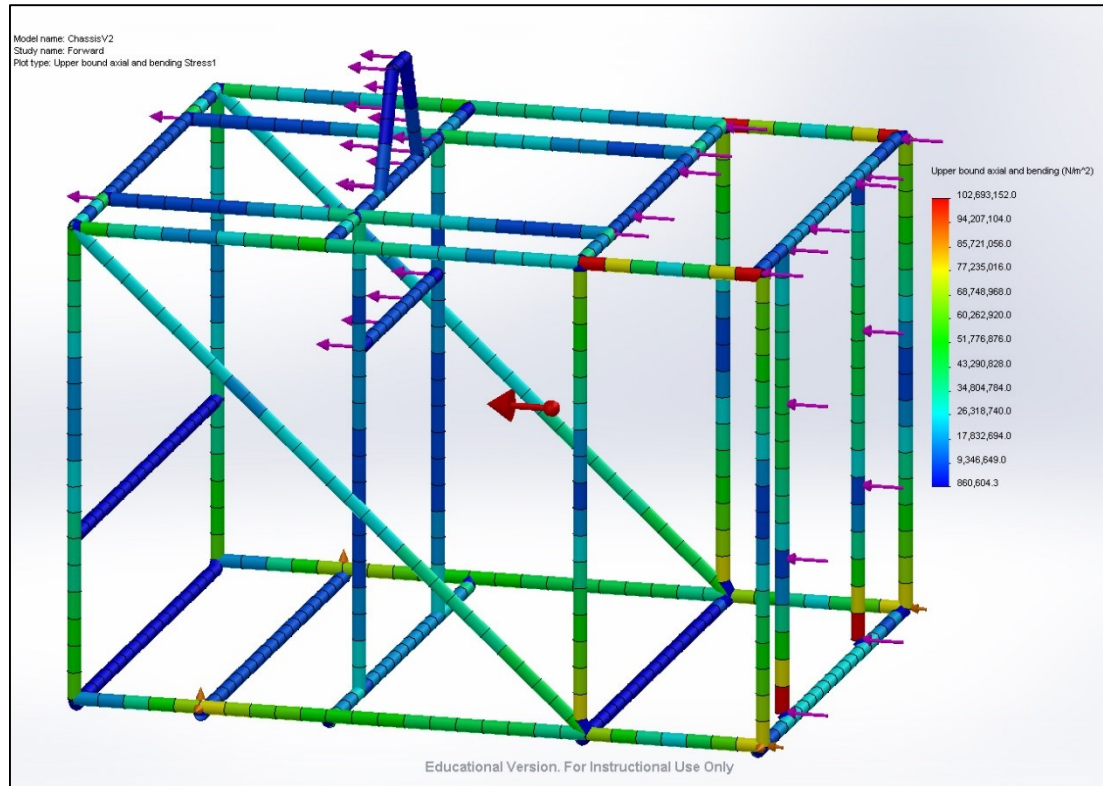
² Not provided by 80/20™ Inc. Loads are assumed double capacity as 2 Hole Corner Gusset. This should be valid for shear force and torsion while conservative for bending stress.

4.3.4 Stress Calculation Methods

In order to evaluate the structural integrity of the payload, the structure was simulated using SolidWorks Simulation (Figure 4.17). Through this simulation, the mass of monitors, haptic devices, robot chambers, computers, the UPS are considered. The values used are shown in Table 4.6. Small components such as the keyboard, E-stops, power strips, and power supplies are not considered because their effect is negligible compared to the loads created by the larger components. Inertial loads of the 80/20™ structure are not considered.

Table 4.6. Component Weights Used for Structural Calculations

Component	Quantity	Unit Mass (kg)
Monitors	5	4.0
Computer	2	11.0
UPS	1	23.6
Haptic Devices	4	2.6
Robot Chamber	1	10.0

**Figure 4.17. SolidWorks Simulation**

Through SolidWorks simulation, peaks stress locations were realized. At these locations, the complex three-dimensional assembly was reduced to simple, conservative two-dimensional structures such as simply-supported and cantilevered beams. Through traditional hand calculations, these conservatively simplified structures are used to prove structural integrity of the entire structure. The hand calculations of the simplified beams are found in the following sections.

When hand calculations are not possible, SolidWorks Simulation was solely. This was required to verify the brackets used to support the monitors and the floor supports used to secure the entire chassis to the aircraft.

4.3.5 Load Cases

Five total load cases for the system are described – Forward, Downward, Lateral, Aft, and Upward. These are calculated by hand using conservative assumptions. The *Upward* and *Aft* load cases are not explicitly calculated because the *Downward* and *Forward* load cases, respectively, are similar in loading but are higher in magnitude. Because elasticity and strengths are assumed to be equivalent for both compressive and tensile loads, the resulting margins will be identical between a compressive load and an equal and parallel tensile load. Therefore, the *Downward* and *Forward* load cases, which have loads in the same direction but with higher magnitudes, will pass the *Upward* and *Aft* load cases by default. Table 4.7 shows a summary of the margins.

Study	Acceleration (g)	Margin
Forward	9.0	58.5%
Downward	6.0	3.3%
Lateral	2.0	-1.0%
Floor Supports	9.0	-22.6%
Monitor Supports	9.0	4.64%

4.3.5.1 Forward

When installed in the aircraft, the forward direction is from the robot container towards the monitors or the positive-z direction as visualized in Figure 4.16. At 9-g this is the most challenging loading condition.

The computers and UPS are loaded onto two beams through the use of standard rack-mount hardware. In this direction, the computers press against the plate. By summing the moments and forces (Figure 4.18), the resultant loads are easily calculated at 600N and 1895N per beam. A bending moment of 331.5 Nm can also be calculated. Referring to Table 4.4, the margin on the strength of the beam can be calculated as seen below. Note that the acceptable moment listed in the table was determined with a safety factor of two. An additional safety factor in the calculation of the safety margin would be redundant and has been removed.

$$\text{Margin} = \frac{608.6}{331.5} - 1 = 85\%$$

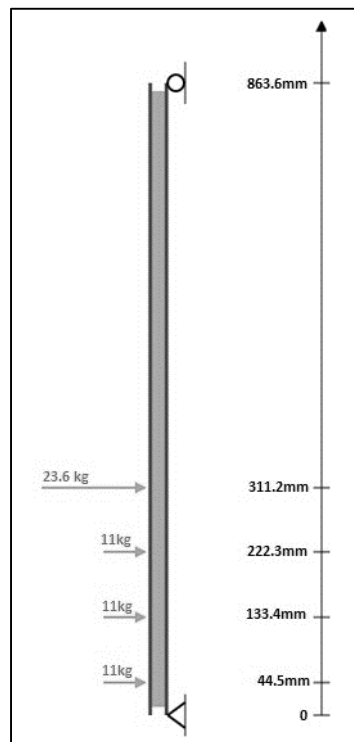


Figure 4.18. Mass and load location of computers and UPS

With the beam passing structurally, the next likely failure point is at the bottom connector. In this particular location, it is assumed that the connector will fail when the T-nuts constraining the connector fail. From Figure 4.19, one can see that five bolts – two in the front and three on the backside – are resisting this load. For clarity, these are circled in red in this figure.

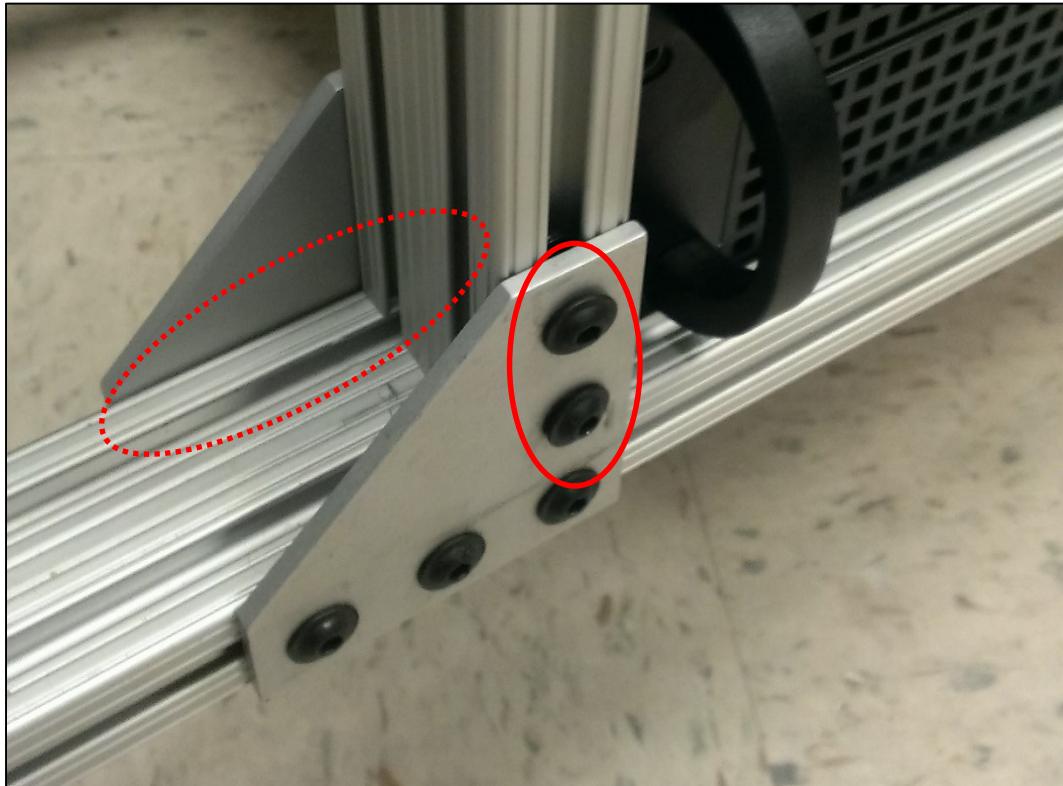


Figure 4.19. Lower brackets of left computer column beam

In order to determine the failure load of the T-nuts, the shear area of the threads is used. From a screw chart, 1/4-20 screws have a pitch diameter of 0.219” and a major diameter of 0.25”. Using the equation below, the shear area and ultimate fastener loads were calculated [52].

$$A = \pi n L D \left(\frac{1}{2n} + 0.57735(D - E) \right)$$

where E = Pitch Diameter of Internal Thread

$D = \text{Major Diameter of External Thread}$

$L = \text{Fastener Engagement, } n = \text{Threads per inch}$

$$A = 0.09389 \text{ in}^2$$

$$F_{ult} = 0.0939 \text{ in}^2 * 33000 \text{ psi} * 0.577 = 1787.95 \text{ lbf} = 7.95 \text{ kN}$$

When the bolts are preloaded to the specified 5 ft-lbf, a force of 3559 N (800 lbf) is achieved [53]. Subtracting this force from the ultimate load of the fasteners gives a working range of 4391 N. From this working range, the minimum number of equally distributed bolts required can be calculated below. For comparison, a margin is also calculated.

$$n = \frac{4391N}{2 * 1895N} = 1.15$$

$$\text{Margin} = \frac{7950N}{3559N + 2 * \left(\frac{1895}{5}\right)} - 1 = 84\%$$

Note that while all five bolts are not likely to carry the load equally, the margin is sufficient to assume structural stability.

During the 9g forward acceleration, the top of the structure will want to translate. With a total of 40.4 kg (monitors, haptic devices, and robot enclosures) at the top of the structure, a force of 1783.5 N per side is applied. When combined with the 600 N reaction from the computers and UPS, a total of 2383 N is experienced per side.

To determine structural integrity against translation, the diagonal 80/20™ beam is assumed to carry all of the load. Using basic statics, the compressive load in this beam will be 3370 N. To ensure that the beam will not buckle, Euler's column buckling equation and the Rankine-Gordon function for medium length beams are used below [53].

$$F_{Euler} = \frac{\pi^2 EI}{(KL)^2} \text{ where } K = 0.65 \text{ (fixed ends)}$$

$$F_{Euler} = 24.98 \text{ kN}$$

$$F_c = Area * \sigma_{yield} = 68.18 \text{ kN}$$

$$F_{max} = \left(\frac{1}{F_{Euler}} + \frac{1}{F_c} \right)^{-1} = 18.28 \text{ kN}$$

$$Margin = \frac{18.28}{2 * 3.37} - 1 = 171\%$$

At the connectors, 3370 N is also experienced. Because 80/20™ connectors will slip at this load, additional measures are taken. A 45° plate uses two fasteners. As calculated previously, these fasteners create a preload force of 3559 N each. From the coefficient of friction between two anodized aluminum surfaces (0.17 from [55]), a friction force of 605 N is available per fastener. Even when using two plates with four fasteners total, this connection will slip.

To combat this, holes are drilled through the 80/20™ beams. This has the advantage of an increased preload (15702N from [54]) as well as a constrained linkage through the plates and the beam where only limited movement is possible even if slippage occurs. Using the rated preload for a standard socket cap screw (15702 N) with a full-size hex nut at the four contact points (two holes per plate, one plate on each side)

$$F_{slip} = 0.17 * 15702 * 4 = 10.68 \text{ kN}$$

$$Margin = \frac{10.68}{2 * 3.37} - 1 = \mathbf{58.5\%}$$

In addition to this margin is the fact that all other connectors were neglected. It is likely that these connectors will carry some portion of these loads as well, further increasing the margin.

4.3.5.2 *Aft*

The calculations for this loading direction are the same as those used for the forward direction with the exception that the diagonal member is in tension instead of compression. Because the forward study passed, it can be safely assumed that the 3g study in the opposite direction passes as well.

4.3.5.3 *Downward*

Highlighted in blue in Figure 4.20 are the downward load areas of concern. The beam on the left is due to the complete load of the five monitors while the beam on the right is due to 50% of the weight of the computers and the UPS. Both of these loads cause bending in a 1" x 1" beam while most other loads are carried axially by vertical beams into a 2" x 1" 80/20™ beam.

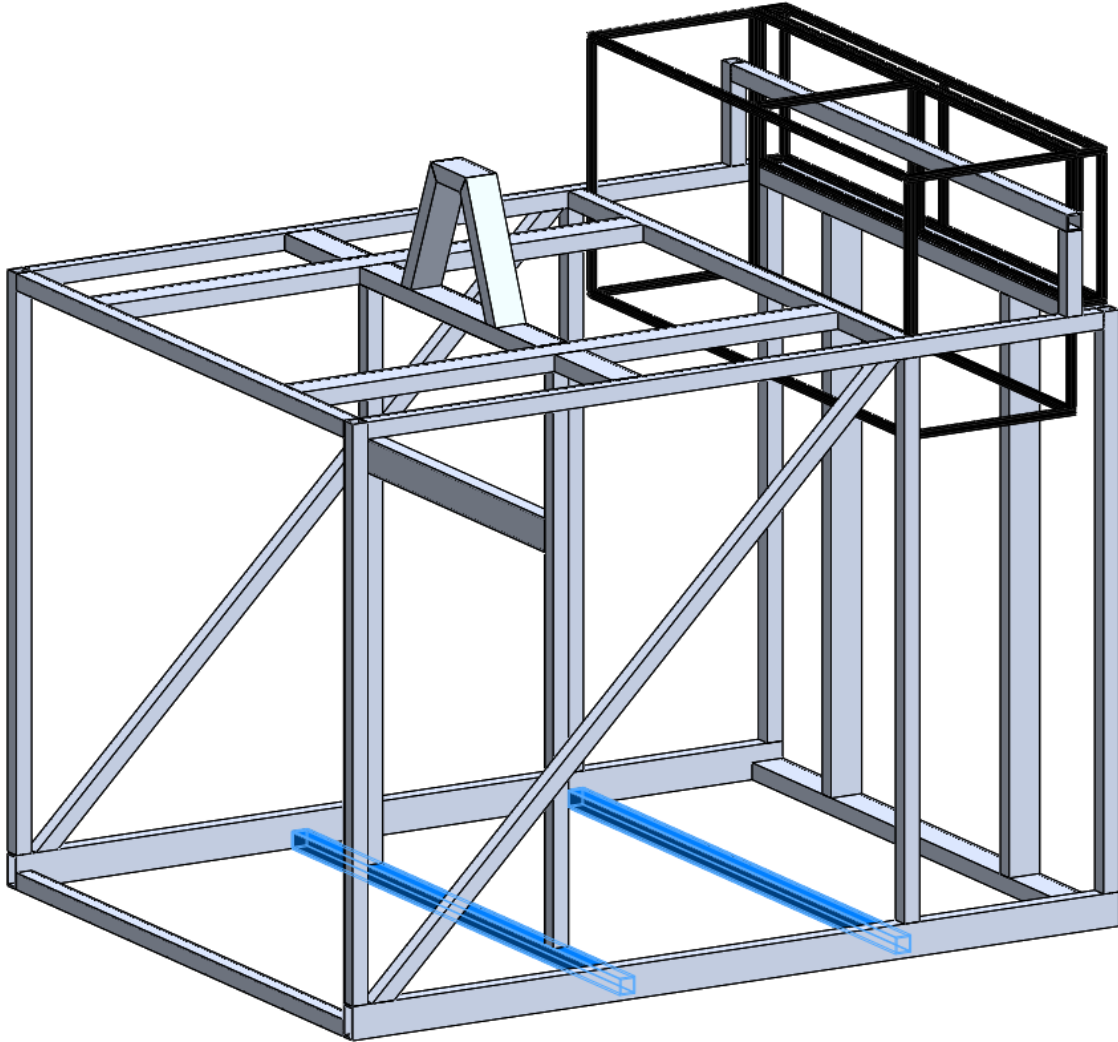


Figure 4.20. Downward load case beams of concern

In analyzing the effect from the monitors, it is assumed that the entire weight is carried down the two vertical columns into the lower beam. At 4kg per monitor in a 6-g environment, the total load in each vertical beam would be 588.6 N. The length of the horizontal beam is 940 mm while the spacing between the central axes of these columns is 533 mm. The equation for the peak moment within a simply supported beam with two symmetric loads is shown below [56].

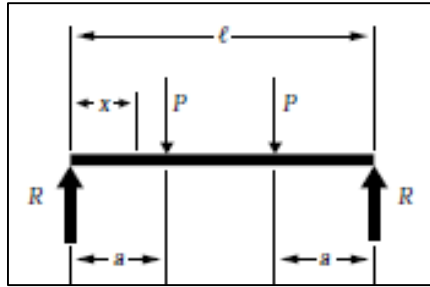


Figure 4.21. Two Symmetrically Spaced Concentrated Loads

$M = P * a$, where $a =$ distance from support to closest load

$$M = 588.6 * 0.203 = 119.6 \text{ Nm}$$

Through Table 4.4,

$$\text{Margin} = \frac{174.8}{119.6} - 1 = 46.2\%$$

Half of the weight of the computers and UPS is carried by the second beam to study (the other half is carried by the double beams to which support the fronts). In summation, the computers and UPS have a total mass of 56.6 kg and it is assumed that the weight of these computers will be applied to the beams at the corners of the cases. By this assumption, the previous equation can also be used.

$M = P * a$, where $a =$ distance from support to closest load

$$M = \frac{50\% * 56.6 \text{ kg} * 9.81 \frac{\text{m}}{\text{s}^2} * 6g's}{2} * 0.203 \text{ m} = 169.24 \text{ Nm}$$

$$\text{Margin} = \frac{174.8}{169.24} - 1 = 3.3\%$$

4.3.5.4 Upward

With the downward load passing sufficiently at 6-g, it can be assumed that the upward load case will also pass. Given that compressive and tensile elasticity and strengths are assumed equal, the margin will be greater than 200 % for an upward acceleration of 2-g.

4.3.5.5 Lateral

From monitors, haptic devices, and the robot enclosure, a total of 40.4 kg of equipment is located at the top of the structure. At 2-g this corresponds to 792.6 N. If the top connectors are assumed to have no rigidity, the problem can be simplified to ten cantilevered beams (neglecting diagonal members) which are fixed through the bottom connectors. At six of these lower joints, double gussets directly prevent angular deflection while the computer column beams are strengthened by a total of four 90° joining plates. In the remaining two joints, single gussets are used. There also exists anchor connectors located at Joints 8 & 11. These, however, are not explicitly rated for moment loads in this direction and are thus ignored.

From the height of the equipment, a moment of 704.7 Nm is generated. The computers and the UPS would generate an additional moment of 230.3 Nm. Through Table 4.5, the summation of acceptable loads for six double gussets, two single gussets, and four 90° joining plates would be 925.2 Nm. The margin on these connectors loaded in this fashion is shown below.

$$\mathbf{Margin} = \frac{925.2}{704.7 + 230.3} - 1 = \mathbf{-1.0\%}$$

Though this margin is negative, it was determined in a very conservative fashion. If the top of the structure were also considered rigid against rotation at the connectors, the strength in each joint would theoretically go up by a factor of four. Because the structure is not fixed against translation and the loading in each beam would not be equal, the strength would not increase by nearly this

much. However, it would increase my some amount. Furthermore, anchor connectors and diagonal members were ignored. Through these points, it can be safely assumed that the connectors satisfy the required safety factor of two.

In analysis of the beams, each 1" x 1" member can carry a load of 174.8 Nm with the safety factor (Table 4.4). In these terms only 5.35 single wide beams would be required to carry this load if the load were distributed equally. In the designed payload, eight 1" x 1" beams and two 1" x 2" beams are used.

4.3.5.6 Floor Supports

The floor supports are milled from 7075-T6 aluminum. They accept four ¼-20 screws which are tightened into 80/20™ T-nuts within an extrusion. Four 3/8" hex cap bolts are then used to secure the supports to the floor.

During the forward 9g load condition, the highest forces are applied to the structure. Because the center of gravity of the payload is above the supports, the weight of the console will induce a moment load in addition to the shear load of the structure. These two loads are set independently in SolidWorks Simulation and their values can be calculated as follows.

$$\textit{Shear} = 1112 \textit{ N} * 9\textit{g}'\textit{s} = 10008 \textit{ N} = \mathbf{2500 \textit{ N per connector horizontally}}$$

$$\textit{Moment} = 10008 \textit{ N} * 0.5 \textit{ (CG Location)} = 5000\textit{Nm} = 2500\textit{Nm per side}$$

$$\textit{Moment} - \textit{induced Force} = \frac{2500\textit{Nm}}{1.016 \textit{ m}} \approx \mathbf{2500 \textit{ N upward or downward}}$$

The results of this simulation are shown in Figure 4.22. During the simulation, the filleted edge shows stress that does not satisfy a safety factor of two. This is not likely realistic due to the simulated infinitely-rigid fixed surface nearby. Nevertheless, a margin is calculated below using

this value. It should be noted that only a small volume is stressed above the safety factor (Figure 4.23) and nothing will yield.

$$\text{Margin} = \frac{505}{2 * 326.2} - 1 = -22.6\%$$

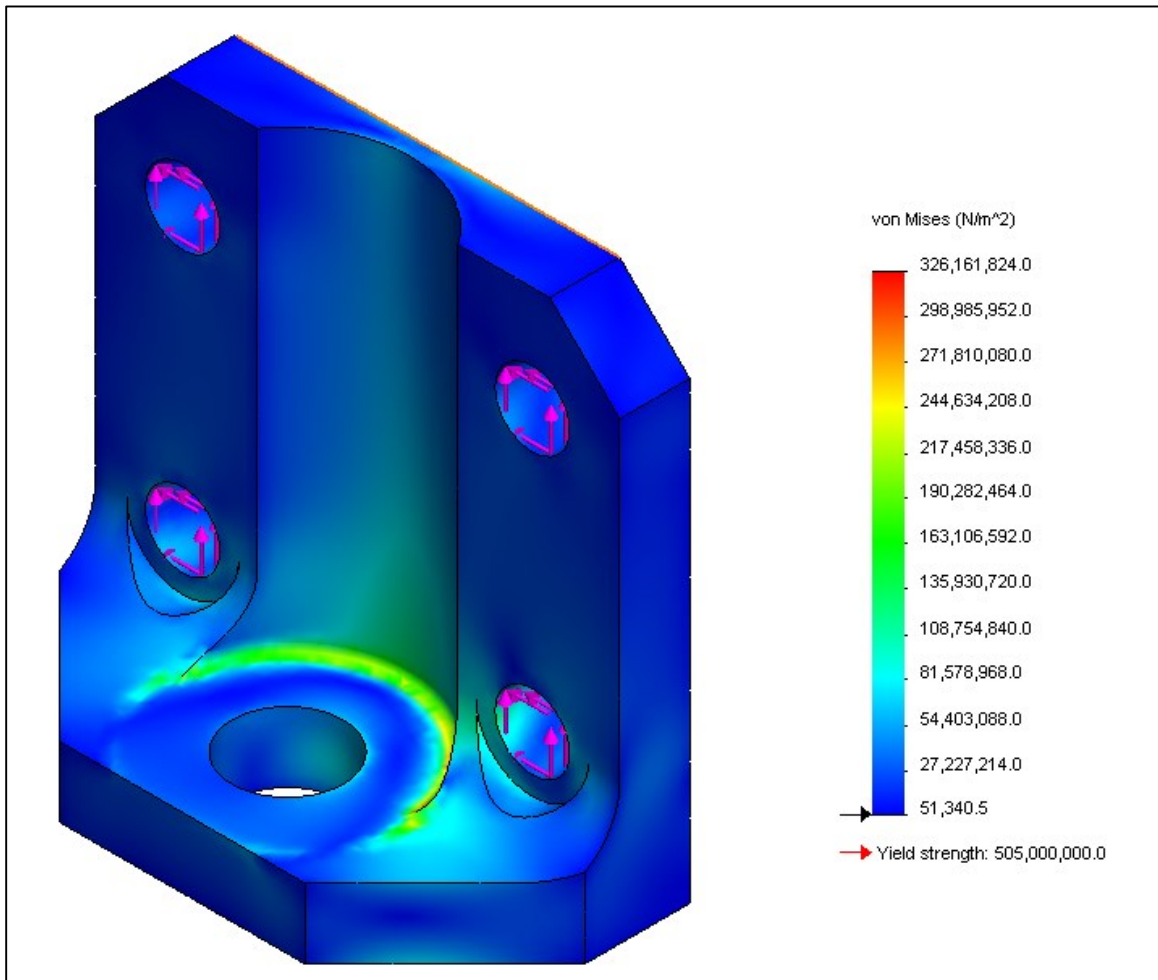


Figure 4.22. Stress Simulation of Floor Supports

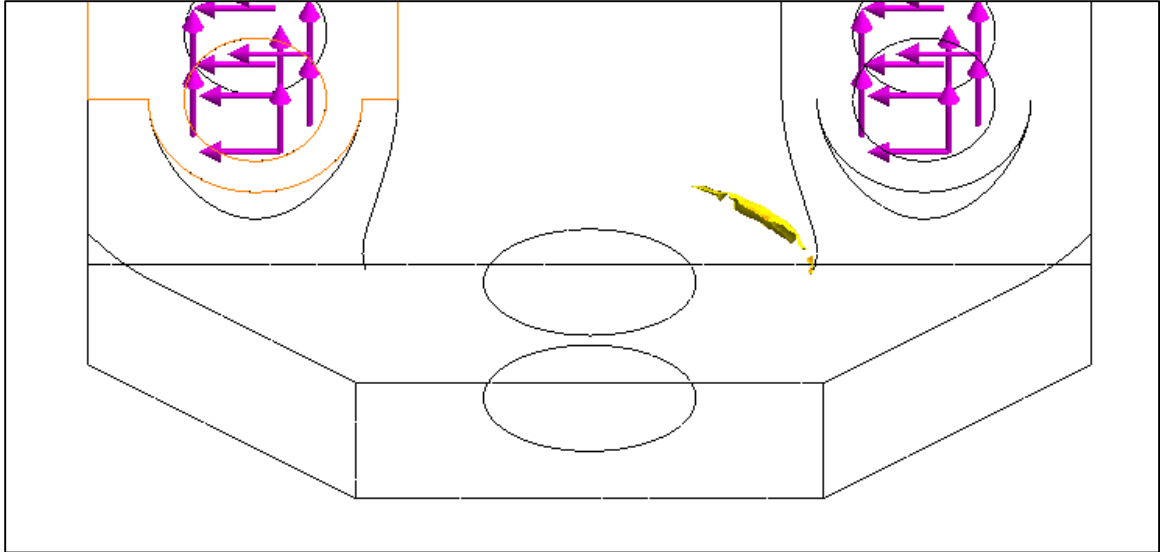


Figure 4.23. Simulation elements with negative safety margins

4.3.5.7 Monitor Supports

To verify the structural integrity of the adapter plates, a remote load equivalent to 9-g (353.16 N) was applied three inches off the face of the plate to account for the center of gravity of the monitor. For the worst case, force was transferred directly to the mounting holes via the rigid purple lines seen in Figure 4.24. The plate was secured by fixing the mating surface of the plate. A 0.75" circle was used for each bolt/washer combination.

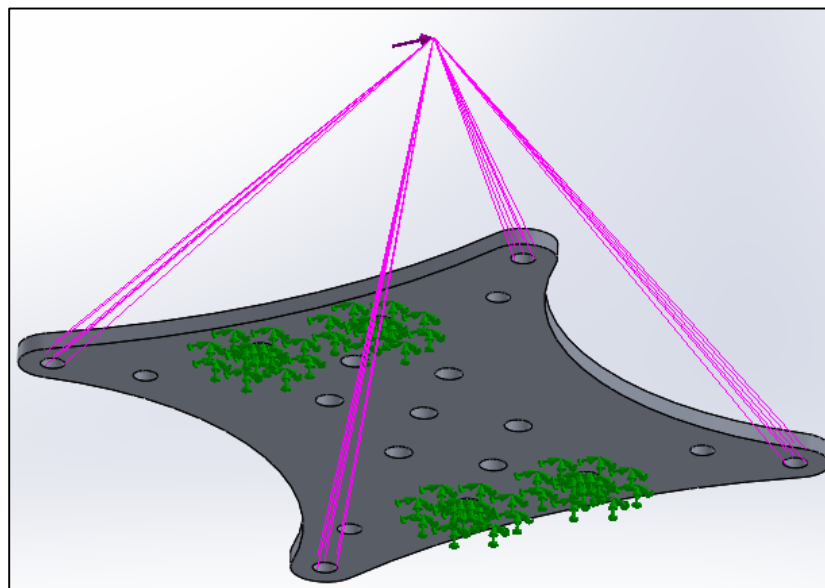


Figure 4.24. Simulation Loading for 80/20™ Monitor Supports

From the simulation a peak stress and corresponding moment were determined and are shown below. The stress distribution can be seen in Figure 4.25.

$$\text{Max Stress} = 131.4 \text{ MPa}$$

$$\text{Margin} = \frac{275}{2 * 131.4} - 1 = 4.64\%$$

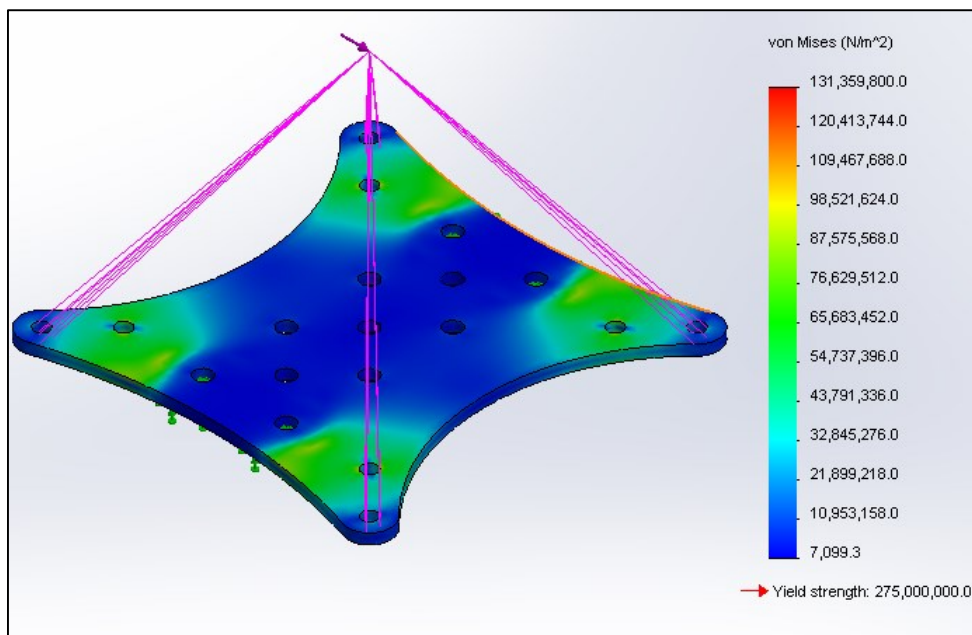


Figure 4.25. Stress Distribution for Monitor Supports

Section 4.4: Electrical Analysis

4.4.1 Load Analysis and UPS Selection

As mentioned previously, a UPS was desired to prevent power fluctuations during operation. A CyberPower OR1500LCDRM2U was chosen as it was capable of supplying electrical loads displayed in Table 4.8. At full load (15A), six minutes of capacity are available while 18 minutes are available at half load. This UPS model has an easily accessible power switch on the front and is rack mountable. An LCD display provides quick status information while RS485/USB output can provide smart shutdown procedures if implemented. While some of the loads in Table 4.8 were measured experimentally, several are specified at the rated input of the power supply which is unlikely to be seen during operation. The overestimate of these components will provide a noticeable margin on the load capacity of this UPS.

Table 4.8. Load Table, 120VAC

Device	Qty:	Current (A)	Total Current (A)
Computers	3	0.87	2.61
Monitors	5	0.44	2.20
Phantom Omni	4	1.2*	4.8*
Network Switch	1	1.0*	1.0*
KVM Switch	1	0.5*	0.5*
HDMI Matrix	1	0.5*	0.5*
Camcorder	4	0.05	0.20
12V Supply	1	1.0*	1.0*
9V Supply	1	1.5*	1.5*
5V Supply	1	0.5*	0.5*
Total			14.81

Note: Devices in Bold were experimentally measured using a Kill A Watt™ EZ electricity load meter at maximum conditions. Computers were run at 100% CPU for 5 minutes while current was measured. Monitors displayed a fully white screen. Camcorders were recording while charging. Values with an asterisk (*) were determined by the rated input of the power supply and will likely be much lower during operation.

4.4.2 Emergency Stops

Two emergency stops will be available to flight members. The first will be an E-stop to kill motor power to the robots. In this fashion, the software systems on both on the robot microcontrollers and on the three Linux computers will not be interrupted. Both robots will be disabled if pressed.

The second E-stop is provided through the power switch located on the front of the UPS. This switch will forcefully shut down all electronics. This will only be used in an extreme case. It should be noted that this does not de-energize the batteries in the UPS.

Chapter 5: Experimental Procedures

This section describes several procedures that must take place prior to, during, and after the microgravity experiment.

1. Ground Operations

While on the ground, casters are to be used for easy movement. These are simply installed with four bolts per wheel. Prior to installation in the aircraft, the casters must be removed. Lift points (Figure 5.1) must be installed at the corners of the assembly.



Figure 5.1. Lift point with handle

Because the payload exceeds 200lb, several components must be removed. These include the monitors and the UPS. The monitors are removed by unscrewing four M3 screws located on the back of each monitor. The UPS is removed through four #8 screws located on the front face of its enclosure. These components will be carried in individually and installed on the aircraft.

While on the ground, the experiment will be set up. This includes placing marked rubber bands in the respective experiment tray, ensuring the robots are fixed securely, and angling cameras to appropriate targets.

2. Loading/Stowing

The experiment will be loaded onto the aircraft by forklift if possible. Once on the plane, the structure will be moved into position by four individuals located at the four corners of the payload. The orientation shown in Figure 5.2 is the orientation used for all directional loading calculations. The experiment will be properly secured to the aircraft floor through the use of four 3/8" steel bolts. Monitors and the UPS will be reinstalled and connected and lift points will be removed. A power cable will be run to the power panel. An extension cord may or may not be necessary.

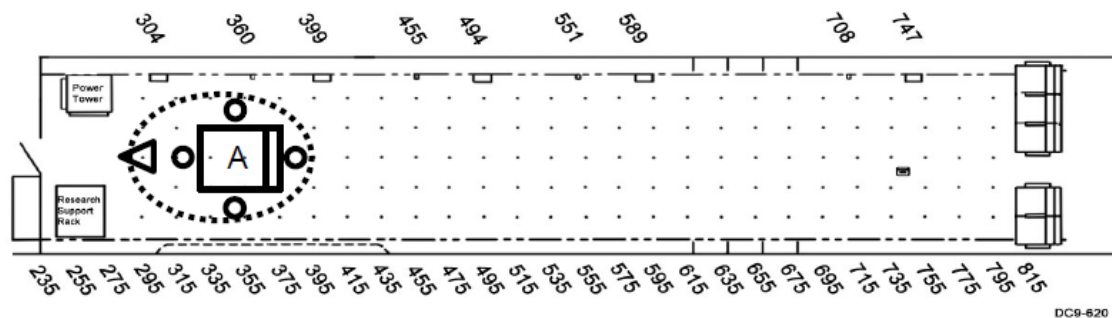


Figure 5.2. Preferred aircraft orientation

Note: The box represents the 80/20™ frame, circles represent operators, and the triangle represents the off-payload camcorder.

Because the stiffness of foam padding in the aircraft is unknown, the foot restraint bars (Figure 5.3) will need to be set to create sufficient downward pressure on the operator's feet to ensure stability. This is accomplished by loosening the $\frac{1}{4}$ -20 screws, sliding the bar downward to the desired level, and then retightening the screws.



Figure 5.3. Foot Restraint Bar (looking downward)

3. Pre-Flight

During pre-flight, ROS will be started and a system initialization will take place. This process will load the communication protocol for the haptic devices and robots and set each device to its proper variable in the system. Camcorders will be turned on but will not be set to record yet. A quick monitor check should take place to ensure each monitor is receiving video from the proper source.

4. Take-off/Landing

During take-off and landing, no operations are required.

5. In-Flight

Prior to experimentation, the robots must be activated. If stowed for take-off, experiments must be loaded into the robot enclosures. Camcorders must be set to record.

While experimenting, one flyer monitors the ROS network through the lower assistant computer. Two operators will be in charge of manipulating the haptic devices to maneuver the robots. These members will be stabilized via the foot straps installed at the base of the payload. The fourth and final flight member will monitor the experiments and the mechanical status of the robots. He may advise the operators throughout the experiments if necessary.

If at some point a crew member gets motion sickness or is injured, the experiment can be performed at full capacity with three people. The robot operator will take a dual role in this scenario. If a second member is incapable of assisting with the flight, both robots can be operated without assistance assuming that no troubleshooting is required.

6. Post-Flight

ROS information will be saved between parabolic flights but camcorders will not. Therefore, camcorders must stop recording and save data. The computers will be safely shut down. Once everything is off, the UPS master switch will cut power to everything it sources and the UPS will be unplugged from the aircraft.

7. Off-Loading

In preparation of unloading, monitors and the UPS will be removed from the structure and will be taken off the plane independently. Lift points will be reinstalled and the structure will be carried by four individuals to the exit. It will be removed from the aircraft via forklift. Casters will be reinstalled once the payload is on hard ground and the experiment will be rolled to the proper staging area.

Chapter 6: Summary

Minimally invasive techniques have shown great capability over the last decade. Through the use of laparoscopic instruments, the quality of health care has greatly improved for the patient at the cost of increased difficulty for the surgeon. Robotic surgical devices assist the surgeon by solving several challenges such as using unintuitive tools and working without tactile feedback or proper depth perception. Whether the device is similar to the *da Vinci*® Surgical System or to the miniature *in vivo* surgical robots developed by the University of Nebraska and mentioned throughout this thesis, robotic surgical systems can greatly improve the medical experience for both the patient and the surgeon.

Long-duration space flight will be attempted at some point in the future. Currently however, there are no viable options for major medical intervention in microgravity; applicants are thoroughly health screened to prevent complications during short missions but this method becomes much less effective for long-duration missions. Through minimally invasive techniques and intuitive controls, surgical robotics show great promise for operation in microgravity environments and should be further developed to do so.



Figure 6.1. Parabolic Flight Payload with EB2.1

Through NASA's Reduced Gravity program, systems developed at the University of Nebraska will be evaluated in a microgravity environment. To carry the experiment, a parabolic flight payload has been developed and assembled (Figure 6.1) and is documented per the requirements of NASA's Reduced Gravity Program [47-50]. The payload design and documentation required for this microgravity research is presented throughout this thesis.

The payload was flown on April 25th, 2014 (Figure 6.2). Two back-to-back flights were completed consisting of 28 zero-gravity parabolas each. Data from these flights is currently being compiled and analyzed to determine if a future flight is necessary. If so, the results of this flight will be very important in developing the second round of experimentation.



Figure 6.2. Experiment performed on April 25th, 2014
Note: Several modifications were made to the payload prior to this experiment

Section 6.1: Future Work

One factor that has inhibited the usability of the robots during *in vivo* testing in standard has been the method of insertion. Currently, the robots are manually inserted using a specialized two-chamber port that maintains insufflation. During this process, a specific series of movements are required to prevent the robot from contacting the organs as it is inserted.

One proposed solution is a gross positioning system with four DOFs about the insertion point – three rotations and one translation. This system would position the body of the robot during insertion prior to surgery, during surgery, and after surgery as the robot is removed. When added to robots with four-DOF arms, the total number of DOFs for the entire system approaches twelve. This creates a robot with six *effective* DOFs per arm without increasing the size of the *in vivo* portion of the robot. Though empirical analysis, this concept has been determined to provide a

sufficient range of tooltip orientations for any point within an equally sized workspace. This addition could greatly reduce the burden of any surgical assistants and would be beneficial in developing a viable system for surgical robots in space.

References

- [1] B. Champagne, J. J. Stulberg, Z. Fan, and C. P. Delaney, “The feasibility of laparoscopic colectomy in urgent and emergent settings,” *Surg. Endosc.*, vol. 23, pp. 1791–1796, 2009.
- [2] C. Zornig, H. Mofid, A. Emmermann, M. Alm, H.-A. von Waldenfels, and C. Felixmüller, “Scarless cholecystectomy with combined transvaginal and transumbilical approach in a series of 20 patients,” *Surg. Endosc.*, vol. 22, pp. 1427–1429, 2008.
- [3] M. S. Liem, Y. van der Graaf, C. J. van Steensel, R. U. Boelhouwer, G. J. Clevers, W. S. Meijer, L. P. Stassen, J. P. Vente, W. F. Weidema, A. J. Schrijvers, and T. J. van Vroonhoven, “Comparison of conventional anterior surgery and laparoscopic surgery for inguinal-hernia repair,” 1997.
- [4] R. Tacchino, F. Greco, and D. Matera, “Single-incision laparoscopic cholecystectomy: surgery without a visible scar,” *Surg. Endosc.*, vol. 23, pp. 896–899, 2009.
- [5] M. J. Mack, “Minimally invasive and robotic surgery,” *JAMA*, vol. 285, pp. 568–572, 2001.
- [6] G. Stiff, M. Rhodes, A. Kelly, K. Telford, C. P. Armstrong, and B. I. Rees, “Long-term pain: less common after laparoscopic than open cholecystectomy,” *Br. J. Surg.*, vol. 81, pp. 1368–1370, 1994.
- [7] J. P. Ruurda, I. A. M. J. Broeders, R. P. M. Simmermacher, I. H. M. Borel Rinkes, and T. J. M. V Van Vroonhoven, “Feasibility of robot-assisted laparoscopic surgery: an evaluation of 35 robot-assisted laparoscopic cholecystectomies,” *Surg. Laparosc. Endosc. Percutan. Tech.*, vol. 12, pp. 41–45, 2002.
- [8] S. Ersin, O. Firat, and M. Sozbilen, “Single-incision laparoscopic cholecystectomy: is it more than a challenge?,” *Surg. Endosc.*, vol. 24, pp. 68–71, 2010.
- [9] G. H. Ballantyne, “Robotic surgery, telerobotic surgery, telepresence, and telementoring. Review of early clinical results,” *Surg. Endosc.*, vol. 16, pp. 1389–1402, 2002.
- [10] F. Corcione, C. Esposito, D. Cuccurullo, A. Settembre, N. Miranda, F. Amato, F. Pirozzi, and P. Caiazzo, “Advantages and limits of robot-assisted laparoscopic surgery: preliminary experience,” 2005.
- [11] K. Moorthy, Y. Munz, A. Dosis, J. Hernandez, S. Martin, F. Bello, T. Rockall, and A. Darzi, “Dexterity enhancement with robotic surgery,” *Surg. Endosc.*, vol. 18, pp. 790–795, 2004.
- [12] R. McCormick, “Six Degree Of Freedom Miniature In Vivo Robot For Laparoendoscopic Single-Site Surgery,” 2011.
- [13] T. D. Wortman, “Design , Analysis , And Testing Of In Vivo Surgical Robots,” 2011.
- [14] J. M. Mondry, “Design and Development of a Four Degree of Freedom In Vivo Surgical Robot for Laparoendoscopic Single-Site Surgery,” 2012.
- [15] T. D. Wortman, A. Meyer, O. Dolghi, A. C. Lehman, R. L. McCormick, S. M. Farritor, and D. Oleynikov, “Miniature surgical robot for laparoendoscopic single-incision colectomy,” *Surgical Endoscopy*, vol. 26. pp. 727–731, 2012.

- [16] S. Horgan and D. Vanuno, "Robots in laparoscopic surgery.," *J. Laparoendosc. Adv. Surg. Tech. A*, vol. 11, pp. 415–419, 2001.
- [17] M. J. Mack, R. J. Aronoff, T. E. Acuff, M. B. Douthit, R. T. Bowman, and W. H. Ryan, "Present role of thoracoscopy in the diagnosis and treatment of diseases of the chest.," *Ann. Thorac. Surg.*, vol. 54, pp. 403–408; discussion 407–409, 1992.
- [18] J. Perissat, D. Collet, and R. Belliard, "Laparoscopic surgery for gallbladder stones.," *Ann. Med.*, vol. 23, pp. 233–236, 1991.
- [19] A. Bell, S.D.Schwaitzberg "Using Vibration to Provide Force Information in Surgery", Tufts University, 2009
- [20] N. Taffinder, S. G. Smith, J. Huber, R. C. Russell, and A. Darzi, "The effect of a second-generation 3D endoscope on the laparoscopic precision of novices and experienced surgeons.," *Surg. Endosc.*, vol. 13, pp. 1087–1092, 1999.
- [21] R. Aggarwal, K. Moorthy, and A. Darzi, "Laparoscopic skills training and assessment.," *Br. J. Surg.*, vol. 91, pp. 1549–1558, 2004.
- [22] B. A. Fransson and C. A. Ragle, "Assessment of laparoscopic skills before and after simulation training with a canine abdominal model.," *J. Am. Vet. Med. Assoc.*, vol. 236, pp. 1079–1084, 2010.
- [23] L. Panait, R. C. Merrell, A. Rafiq, S. J. Dudrick, and T. J. Broderick, "Virtual Reality Laparoscopic Skill Assessment in Microgravity," *J. Surg. Res.*, vol. 136, pp. 198–203, 2006.
- [24] H.-J. Han, S.-B. Choi, W.-B. Kim, and S.-Y. Choi, "Single-incision multiport laparoscopic cholecystectomy: things to overcome.," *Arch. Surg.*, vol. 146, pp. 68–73, 2011.
- [25] K. Ahmed, T. T. Wang, V. M. Patel, K. Nagpal, J. Clark, M. Ali, S. Deeba, H. Ashrafian, A. Darzi, T. Athanasiou, and P. Paraskeva, "The role of single-incision laparoscopic surgery in abdominal and pelvic surgery: a systematic review.," *Surg. Endosc.*, vol. 25, pp. 378–396, 2011.
- [26] H. Ross, S. Steele, M. Whiteford, S. Lee, M. Albert, M. Mutch, D. Rivadeneira, and P. Marcello, "Early multi-institution experience with single-incision laparoscopic colectomy.," *Dis. Colon Rectum*, vol. 54, pp. 187–192, 2011.
- [27] C. Delany, P. Neary, A. Heriot and A. Senagore, *Operative Techniques in Laparoscopic Colorectal Surgery*, Philadelphia: Lippincott Williams & Wilkins, 2007.
- [28] M. M. Desai, A. K. Berger, R. Brandina, M. Aron, B. H. Irwin, D. Canes, M. R. Desai, P. P. Rao, R. Sotelo, R. Stein, and I. S. Gill, "Laparoscopic Single-site Surgery: Initial Hundred Patients," *Urology*, vol. 74, pp. 805–812, 2009.
- [29] P. F. Escobar, D. Starks, A. N. Fader, M. Catenacci, and T. Falcone, "Laparoscopic single-site and natural orifice surgery in gynecology," *Fertil. Steril.*, vol. 94, pp. 2497–2502, 2010.
- [30] A. N. Fader and P. F. Escobar, "Laparoscopic single-site surgery (LESS) in gynecologic oncology: Technique and initial report," *Gynecol. Oncol.*, vol. 114, pp. 157–161, 2009.

- [31] D. B. Camarillo, T. M. Krummel, and J. K. Salisbury, "Robotic technology in surgery: Past, present, and future," *American Journal of Surgery*, vol. 188, 2004.
- [32] H. W. R. Schreuder and R. H. M. Verheijen, "Robotic surgery.," *BJOG*, vol. 116, pp. 198–213, 2009.
- [33] S. DiMaio, M. Hanuschik, and U. Kreaden, "The da Vinci Surgical System," in *Surgical Robotics: Systems Applications and Visions*, 2011, pp. 199–217.
- [34] B. Hannaford, J. Rosen, D. W. Friedman, H. King, P. Roan, L. Cheng, D. Glozman, J. Ma, S. N. Kosari, and L. White, "Raven-II: an open platform for surgical robotics research.," *IEEE Trans. Biomed. Eng.*, vol. 60, pp. 954–9, 2013.
- [35] X. Zhang, D. Oleynikov, and C. A. Nelson, "Portable tool positioning robot for telesurgery.," *Stud. Health Technol. Inform.*, vol. 142, pp. 438–443, 2009.
- [36] N. Zemiti, G. Morel, T. Ortmaier, and N. Bonnet, "Mechatronic Design of a New Robot for Force Control in Minimally Invasive Surgery," *IEEE/ASME Trans. Mechatronics*, vol. 12, 2007.
- [37] U. Hagn, R. Konietzke, A. Tobergte, M. Nickl, S. Jörg, B. Kübler, G. Passig, M. Gröger, F. Fröhlich, U. Seibold, L. Le-Tien, A. Albu-Schäffer, A. Nothhelfer, F. Hacker, M. Grebenstein, and G. Hirzinger, "DLR MiroSurge: a versatile system for research in endoscopic telesurgery.," *Int. J. Comput. Assist. Radiol. Surg.*, vol. 5, pp. 183–193, 2010.
- [38] A. M. Okamura, "Haptic feedback in robot-assisted minimally invasive surgery.," *Curr. Opin. Urol.*, vol. 19, pp. 102–107, 2009.
- [39] J. Rosen, M. Lum, M. Sinanan, and B. Hannaford, "Raven: Developing a Surgical Robot from a Concept to a Transatlantic Teleoperation Experiment," in *Surgical Robotics SE - 8*, 2011, pp. 159–197.
- [40] R. H. Taylor, "A Perspective on Medical Robotics," *Proc. IEEE*, vol. 94, 2006.
- [41] J.R. Bartels, "Development of Distributed Motor Control and Haptic Feedback Systems for Miniature in vivo Surgical Robots," 2013.
- [42] M. R. Campbell, R. D. Billica, R. Jennings, and S. Johnston, "Laparoscopic surgery in weightlessness.," *Surg. Endosc.*, vol. 10, pp. 111–117, 1996.
- [43] L. Panait, T. Broderick, A. Rafiq, J. Speich, C. R. Doarn, and R. C. Merrell, "Measurement of laparoscopic skills in microgravity anticipates the space surgeon.," *Am. J. Surg.*, vol. 188, no. 5, pp. 549–52, Nov. 2004.
- [44] A. Rafiq, R. Hummel, V. Lavrentyev, W. Derry, D. Williams, and R. C. Merrell, "Microgravity effects on fine motor skills: tying surgical knots during parabolic flight.," *Aviat. Space. Environ. Med.*, vol. 77, pp. 852–856, 2006.
- [45] A. W. Kirkpatrick, D. Hamilton, D. Short, M. R. Campbell, R. Jennings, R. D. Billica, S. A. Dulchavsky, and S. L. Johnston, "Endoscopic surgery in weightlessness," *Surg. Endosc.*, vol. 15, pp. 1413–1418, 2001.
- [46] E.J.Markvicka, T.P. Frederick, K.M. Lackas, S.M. Farritor, Miniature in vivo surgical robot for space applications, NASA Human Research Program Investigators' Workshop, 2014

- [47] National Aeronautics and Space Administration, AOD33896, Test Equipment Data Package Requirement and Guidelines, 2010
- [48] National Aeronautics and Space Administration, AOD33897, Experiment Design Requirements and Guidelines for Microgravity Research, 2013
- [49] National Aeronautics and Space Administration, AOD33899, JSC Reduced Gravity Program User's Guide, 2013
- [50] National Aeronautics and Space Administration, AOD33912, Interface Control Document, 2011
- [51] E. M. Markvicka, Design and Development of a Four Degree of Freedom In Vivo Surgical Robot for Laparoendoscopic Single-Site Surgery, 2014.
- [52] Fastenal Engineering and Design Support, Screw Thread Design, 2009
- [53] R. G. Budynas, J. K. Nisbett, Shigley's Mechanical Engineering Design, 2011
- [54] Holo-Krome, Technical Handbook, 2008
- [55] SIS Handbook, Aluminum, ed. 3, June 2003
- [56] Beam Design Formulas with Shear and Moment Diagrams, American Wood Council, Design Aid No. 6, 2007
- [57] 80/20™ Catalog 18, 80/20™ Inc, 2012

Appendix A: 80/20™ Datasheets

80/20® Inc.
The Industrial Erector Set®
THE STANDARD

Simple Beam Deflection Calculations

Use the formulas listed below to find the worst case deflection for a beam:

Formula A

$$\frac{L^3 \cdot W}{48 \cdot E \cdot I} = D$$



This formula will yield worst case deflection for a beam supported at both ends with the load centered over the span.

Formula B

$$\frac{5L^3 \cdot W}{384 \cdot E \cdot I} = D$$



This formula will yield worst case deflection for a beam supported at both ends with the load evenly distributed over the span.

Formula C

$$\frac{L^3 \cdot W}{3 \cdot E \cdot I} = D$$



This formula will yield worst case deflection for a beam fastened at one end and cantilevered horizontally with the load applied at the end of the beam.

1

Example Using Formula A:

Using the 1515 T-slotted profile, a length of 30.0", and an applied force of 50 lbs., you should find the approximate beam deflection to be .011".

Formula Reference:

L = Length in Inches
E = Modulus of Elasticity (10,200,000)
I = Moment of Inertia (see material specifications on pages 68-69)

W = Load in Pounds
D = Deflection in Inches

Fractional Profile Standards

- Yield strength 35,000 lbs. /sq. in. minimum
- Tensile strength 38,000 lbs. /sq. in. minimum
- Elongation A5 minimum 10%
- Elongation A10 minimum 8%
- Elasticity E approximately 10,200 k lbs./sq.in.
- Rockwell hardness approximately E-88
- Extrusion conforming to DIN 17 615 specifications
- Twist per foot of length not to exceed .25 degree and total twist over 20 feet of length not to exceed 1.5 degrees
- Flatness .004" per inch of width
- Straightness 0.0125" per foot of length, not to exceed .120" over 20 feet of length
- Unless otherwise specified, all profiles will have etch and clear (MIL-A-8625F) anodizing with depth of .0004" and surface hardness of approximately 250 HV (anodized profiles should not be welded because of toxic fumes)

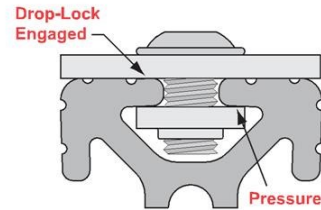
154

We specialize in **FAST™** same day shipments!

Fractional

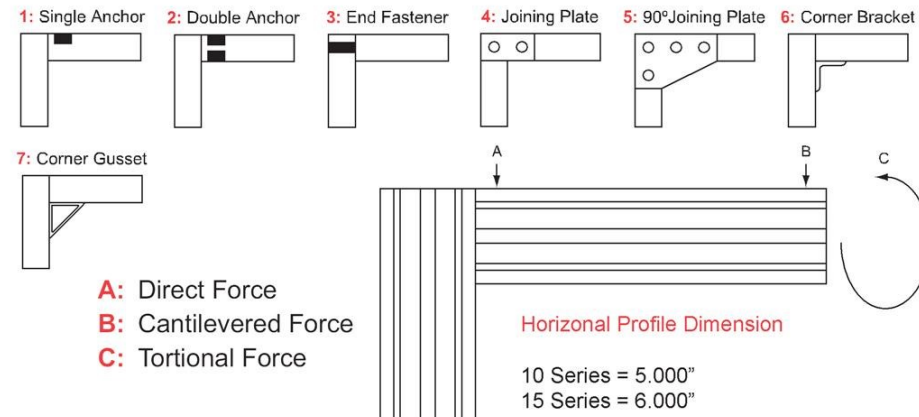
Torque Specifications

- See table below for the amount of torque in foot-lbs. required to activate the 2° drop-lock feature for T-slotted profiles
- Nut and bolt combination is pre-loaded when tightened to the minimum torque rating
- When properly tightened, fasteners will not loosen even under heavy vibration



Part Number	Fastener Description	Tested Profile	Minimum Ft.-lbs. Torque	Maximum Ft.-lbs. Torque
3320	5/16-18 x 11/16 Flanged BHSCS & Economy T-Nut	1515	10.00	15.00
3325	5/16-18 x 3/4 Economy T-Slot Stud, Washer & Hex Nut	1515	30.00	40.00
3360	15 Series Anchor Fastener Assembly	1515-Lite	10.00	28.00
3380	15 Series End Fastener Assembly	1515-Lite	10.00	22.00
3321	1/4-20 x 1/2 Flanged BHSCS & Economy T-Nut	1010	4.00	6.00
3395	10 Series Anchor Fastener Assembly	1010	3.00	17.00
3381	10 Series End Fastener Assembly	1010	4.00	17.00

Fastener Application Tests



Fastener	1010 Profile			1515-Lite Profile			1515 Profile		
	A (lbs.)	B (lbs.)	C (Inch.-lbs.)	A (lbs.)	B (lbs.)	C (Inch.-lbs.)	A (lbs.)	B (lbs.)	C (Inch.-lbs.)
1	500	250	180	950	625	540	950	1,000	700
2	900	250	260	1,200	700	1,150	1,200	1,200	2,000
3	450	200	325	1,000	500	680	1,000	820	1,150
4	175	50	400	225	200	1,000	225	200	1,100
5	175	50	500	250	200	1,120	250	200	1,260
6	325	75	180	375	225	500	575	225	500
7	325	220	260	375	750	500	575	750	500

Note: Plates, brackets and gussets were attached with 80/20[®] recommended bolt kits. Fasteners were tightened according to 80/20[®] torque specifications found at the top of the page.

Test results reflect the connection failure point. Loads at or above these points are not recommended.

Phone: 260-248-8030 • Fax: 260-248-8029 • www.8020.net

Fractional

1010 T-Slotted Profile - 10 Series

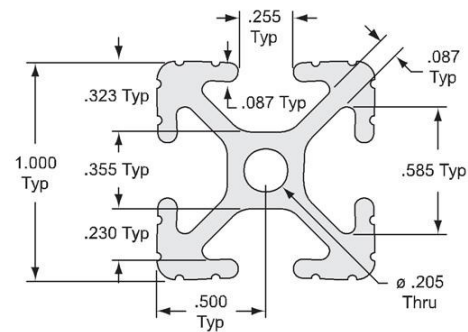
- Compatible with all 10 Series fasteners
- Four open T-slots for mounting accessories
- 1010 is ideal for machine guards, sound enclosures, work benches, displays and panel mount racks
- Compatibility Code*: 6-10



**VIBRATION
PROOF™**

1

Part No.	1010
Material	6105-T5
Finish	Clear Anodized
Weight Per Foot	.5097 Lbs.
Stock Length (+/- .125")	97" - Part No. 1010-97 145" - Part No. 1010-145 242" - Part No. 1010-242
Moment Of Inertia	IX=.0442 ⁱⁿ⁴ IY=.0442 ⁱⁿ⁴
Estimated Area	.4379 Sq. In.



Quick Machining Reference

Machining Service	Service Number
Cut to Length	7005 (see page 563)
.218" Access Hole	7051 (see page 565)
Anchor Counterbore	7042 (see page 567)
Tap Profile End	7061 (see page 564)

Pre-Cut Lengths

48" - Part No. **1010-48** 72" - Part No. **1010-72**

- Pre-cut, ready to ship
- Cut to our standard tolerance of +/- .015"
- One part number, one price (includes cut charge)

Note: Look for the  icon throughout the Fractional portion of this catalog. This icon points out all 10 Series compatible parts and accessories.

* See Compatibility Code information on page 152.

** See 2° Drop-Lock information on page 150.

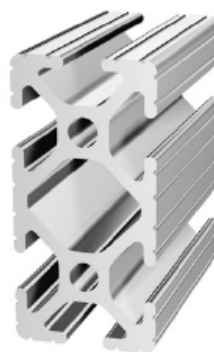
Phone: 260-248-8030 • Fax: 260-248-8029 • www.8020.net

159

Fractional

1020 T-Slotted Profile - 10 Series

- Compatible with most 10 Series fasteners
- Six open T-slots for mounting accessories
- The center cavity can be pressurized up to 150 psi; refer to pages 451-453
- Ideal for machine guards, sound enclosures, work benches, displays and panel mount racks
- Compatibility Code*: 6-10




VIBRATION
PROOF™**

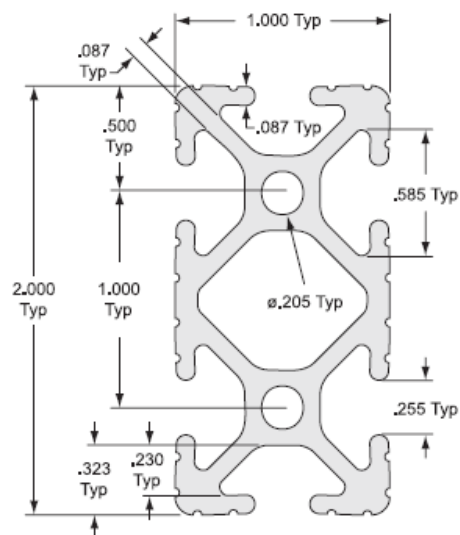
1

Part No.	1020
Material	6105-T5
Finish	Clear Anodized
Weight Per Foot	.9212 Lbs.
Stock Length (+/- .125")	97" - Part No. 1020-97 145" - Part No. 1020-145 242" - Part No. 1020-242
Moment Of Inertia	IX=.3078** IY=.0833**
Estimated Area	.7914 Sq. In.

Quick Machining Reference

Machining Service	Service Number
Cut to Length	7000 (see page 563)
.218" Access Hole	7051 (see page 565)
Anchor Counterbore	7042 (see page 567)
Tap Profile End	7046 (see page 564)

Note: Look for the  icon throughout the Fractional portion of this catalog. This icon points out all 10 Series compatible parts and accessories.



Pre-Cut Lengths 48" - Part No. **1020-48** 72" - Part No. **1020-72**

- Pre-cut, ready to ship
- Cut to our standard tolerance of +/- .015"
- One part number, one price (includes cut charge)

* See Compatibility Code information on page 150.

** See 2" Drop-Lock information on page 150.

Phone: 260-248-8030 • Fax: 260-248-8029 • www.8020.net

167